2015

Deconvoluting heme biosynthesis to target blood-stage malaria parasites

Paul A. Sigala
Washington University School of Medicine in St. Louis

Jan R. Crowley
Washington University School of Medicine in St. Louis

Jeffrey P. Henderson
Washington University School of Medicine in St. Louis

Daniel E. Goldberg
Washington University School of Medicine in St. Louis

Deconvoluting heme biosynthesis to target blood-stage malaria parasites

Paul A Sigala, Jan R Crowley, Jeffrey P Henderson, Daniel E Goldberg

DOI: http://dx.doi.org/10.7554/eLife.09143

Cite as: eLife 2015;10.7554/eLife.09143

Received: 2 June 2015
Accepted: 13 July 2015
Published: 14 July 2015

Deconvoluting Heme Biosynthesis to Target Blood-Stage Malaria Parasites

Paul A. Sigala[1,2], Jan R. Crowley[3], Jeffrey P. Henderson[1-3], and Daniel E. Goldberg[1,2*]

[1]Department of Molecular Microbiology, [2]Department of Medicine Division of Infectious Diseases, and [3]Center for Women's Infectious Disease Research, Washington University School of Medicine, St. Louis, MO 63110.
[*]Email: goldberg@wusm.wustl.edu

Competing interests statement. P.A.S. and D.E.G. are co-inventors on a provisional patent application entitled "Combination Artemisinin and Chemiluminescent Photodynamic Therapy and Uses Therefor".

Abstract

Heme metabolism is central to blood-stage infection by the malaria parasite, *Plasmodium falciparum.* Parasites retain a heme biosynthesis pathway but do not require its activity during infection of heme-rich erythrocytes, where they can scavenge host heme to meet metabolic needs. Nevertheless, heme biosynthesis in parasite-infected erythrocytes can be potently stimulated by exogenous 5-aminolevulinic acid (ALA), resulting in accumulation of the phototoxic intermediate, protoporphyrin IX (PPIX). Here we use photodynamic imaging, mass spectrometry, parasite gene disruption, and chemical probes to reveal that vestigial host enzymes in the cytoplasm of *Plasmodium*-infected erythrocytes contribute to ALA-stimulated heme biosynthesis and that ALA uptake depends on parasite-established permeability pathways. We show that PPIX accumulation in infected erythrocytes can be harnessed for antimalarial chemotherapy using luminol-based chemiluminescence and combinatorial stimulation by low-dose artemisinin to photoactivate PPIX to produce cytotoxic reactive oxygen. This photodynamic strategy has the advantage of exploiting host enzymes refractory to resistance-conferring mutations.

Introduction

Malaria is an ancient and deadly scourge of humanity, with hundreds of millions of people infected by *Plasmodium* malaria parasites and more than 600,000 deaths each year.[1] Substantial progress has been made in reducing the global malaria burden, due in part to the success of artemisinin-based combination drug therapies (ACTs). Recent identification of artemisinin-tolerant parasites in southeast Asia, however, has raised concerns that the broad potency of ACTs against all parasite strains may be waning, which could lead to a resurgence in malaria deaths.[2,3] These concerns motivate continued efforts to deepen understanding of basic parasite biology in order to identify new drug targets and facilitate development of novel therapies.

Heme is a ubiquitous biological cofactor required by nearly all organisms to carry out diverse redox biochemistry.[4] Heme metabolism is a dominant feature during *Plasmodium* infection of erythrocytes, the most heme-rich cell in the human body and the stage of parasite development that causes all clinical symptoms of malaria. Parasites sequester and biomineralize the copious heme released during large-scale hemoglobin digestion in their acidic food vacuole,[5,6] but they also require heme as a metabolic cofactor for cytochrome-mediated electron transfer within mitochondria.[5-7]

Sequencing of the *P. falciparum* genome over a decade ago and subsequent studies have revealed that parasites encode and express all of the conserved enzymes for a complete heme biosynthesis pathway (Figure 1a), but the role and properties of this pathway have been the subject of considerable confusion and uncertainty.[5,6,8] This pathway was originally proposed to be essential for blood-stage parasite development and thus a potential drug target,[9] as host heme was thought to be inaccessible for parasite utilization in mitochondria. Recent studies, however,

have clarified that *de novo* heme synthesis is not required by intraerythrocytic parasites and therefore is unlikely to be a viable target for therapeutic inhibition.[10,11] The parasite-encoded ferrochelatase (FC) can be knocked out to ablate heme biosynthesis but parasite growth is unaffected, suggesting that parasites can scavenge host heme to satisfy metabolic requirements during blood-stage infection.

Here we use chemical and physical probes to decipher the role of upstream enzymes in heme biosynthesis by parasite-infected erythrocytes. Contrary to simple predictions, genetic disruption of the parasite porphobilinogen deaminase (PBGD) and coproporphyrinogen III oxidase (CPO) had no effect on the ability of *Plasmodium*-infected erythrocytes to convert exogenous ALA into heme, as monitored by mass spectrometry and photodynamic imaging of porphyrin intermediates. Biochemical fractionation revealed that vestigial host enzymes remaining in the erythrocyte cytoplasm contribute to ALA-stimulated heme biosynthesis, explaining why disruption of parasite enzymes had no effect on biosynthetic flux. We used small-molecule probes to show that ALA uptake by erythrocytes, which are normally impermeable to ALA, requires the parasite nutrient acquisition pathways established after invasion. Finally, we show that latent host enzyme activity can be exploited for antimalarial photodynamic therapy, using 1) ALA to stimulate production of phototoxic PPIX, 2) luminol-based chemiluminescence to photoactivate PPIX cytotoxicity within infected erythrocytes, and 3) luminol stimulation by combinatorial low-dose artemisinin.

Results

Exogenous ALA stimulates heme biosynthesis and photosensitizes parasites. Production of 5-aminolevulinic acid (ALA) by ALA synthase (ALAS) is the regulated step in heme biosynthesis. Exogenous ALA bypasses this step and stimulates biosynthetic flux, leading to accumulation of the final intermediate, protoporphyrin IX (PPIX), since conversion of PPIX to heme by ferrochelatase becomes rate limiting.[12] PPIX is fluorescent (Figure 1- figure supplement 1) and its cellular accumulation can be directly visualized by fluorescence microscopy, a phenomenon called photodynamic imaging that has been exploited for visualizing cancerous tumor boundaries during surgical resection.[13]

Prior work indicated that exogenous ALA stimulates PPIX production in *P. falciparum* parasites.[10,14] We therefore posited that ALA treatment could serve as a probe of heme biosynthesis activity in *Plasmodium*-infected erythrocytes by enabling direct visualization of PPIX production and the cellular consequences of light activation. Untreated parasites imaged on an epifluorescence microscope display only background auto-fluorescence from hemozoin crystals in the parasite digestive vacuole (Figure 1b). Parasites grown in 200 μM ALA, however, display bright red fluorescence distributed throughout the infected erythrocyte, as expected for accumulation of PPIX (Figure 1b).

PPIX is also known to generate cytotoxic reactive oxygen species when photo-illuminated, due to formation of an excited triplet state that can undergo collisional energy transfer with ground state triplet oxygen to produce highly reactive singlet oxygen.[13] The ability to kill ALA-treated cells by light activation of accumulating PPIX has been exploited to selectively target cancerous tumors via a strategy known as photodynamic therapy.[12,13]

The cytotoxic effects of light-activating PPIX were readily apparent by monitoring the motion of hemozoin crystals that dynamically tumble within the digestive vacuole of individual parasites. Although the origin and physiological significance of this motion remain unknown, hemozoin dynamics serve as an internal biomarker of food vacuole integrity and parasite viability.[5] Hemozoin motion in untreated parasites was unaffected by exposure to light that overlaps the excitation wavelength of PPIX (Videos 1 and 2). In contrast, the hemozoin dynamics in ALA-treated parasites were rapidly ablated by light (Videos 3 and 4). Ultra-structural analysis by electron microscopy revealed a loss of electron density within the digestive vacuole of ALA-treated and illuminated parasites (Figure 1- figure supplement 2), suggesting disruption of the food vacuole membrane and outward diffusion of the vacuolar protein contents. These changes are consistent with a photodynamic mechanism of PPIX-mediated generation of reactive oxygen species that cause pleiotropic cytotoxic damage, including loss of lipid bilayer integrity.

To test the effects of these changes on bulk parasite culture, we monitored the growth of untreated versus ALA-treated parasites over several days with 2-minute daily exposures to broad-wavelength white light on an overhead projector light box. Whereas untreated parasite cultures grew normally in the presence of light, the growth of ALA-treated cultures was strongly attenuated by light (Figure 1c and Figure 1- figure supplement 3), consistent with a prior report.[14] Microscopic examination by blood smear revealed that ALA-treated cultures predominantly contained karyolytic and pyknotic parasites (Figure 1- figure supplement 4), indicative of widespread cell death. The photosensitivity of parasite growth in ALA was fully rescued by 50 μM succinylacetone (SA), an ALA dehydratase (ALAD) inhibitor shown in previous work to substantially reduce PPIX biosynthesis from ALA in parasite-infected

erythrocytes.[10,11] This chemical rescue confirmed that parasite photosensitivity in ALA requires biosynthetic conversion of ALA to PPIX.

Stable disruption of parasite enzymes or the apicoplast organelle does not affect heme biosynthesis from ALA. The constituent enzymes of the parasite's heme biosynthesis pathway are distributed between three sub-cellular compartments: the mitochondrion, the cytoplasm, and the chloroplast-like but non-photosynthetic apicoplast organelle (Figure 1a).[6] Prior work indicated that the parasite ferrochelatase gene could be knocked out, resulting in a complete ablation of *de novo* heme synthesis but with no effect on parasite growth.[10,11] This observation provided strong evidence that parasites do not require heme biosynthesis for growth in erythrocytes, where they can presumably scavenge abundant host heme to meet metabolic needs. We therefore reasoned that upstream enzymes in the parasite-encoded heme biosynthesis pathway should also be amenable to genetic disruption and that such ablations would block production of PPIX from exogenous ALA (Figure 1a) and thus prevent parasite photosensitivity.

We successfully disrupted the parasite genes encoding the apicoplast-targed porphobilinogen deaminase (PBGD) (Figure 2- figure supplement 1) and the cytosolic coproporphyrinogen III oxidase (CPO) (Figure 2- figure supplement 2), using single-crossover homologous recombination to truncate the open reading frame for each gene. Southern blot and PCR analysis confirmed correct integration and gene disruption in clonal parasite lines (Figure 2-figure supplements 3 and 4). Contrary to simple predictions, however, these genetic disruptions had no effect on the ability of parasite-infected erythrocytes to incorporate ^{13}C-labelled ALA into heme, PPIX, or coproporphyrinogen III (Figure 2a), as monitored by a previously developed

184 liquid chromatography-tandem mass spectrometry (LC-MS/MS) assay,[10] and clonal growth of
185 both parasite lines remained fully photosensitive in ALA (Figure 2b,c).

186 To further probe the functional contributions to heme biosynthesis by the parasite
187 apicoplast and its constituent enzymes, we stably disrupted this organelle by treating parasites
188 with doxycycline and isopentenyl pyrophosphate (IPP). Doxycycline inhibits the prokaryotic
189 translation machinery of the apicoplast, which blocks replication of the small apicoplast genome,
190 prevents organelle segregation, and results in unviable apicoplast-deficient parasite progeny.[15]
191 The lethal effects of doxycycline, however, can be chemically rescued by IPP, which enables
192 parasites to make essential isoprenoids despite apicoplast disruption and leads to a stable
193 metabolic state in which parasites lack the intact organelle such that nuclear-encoded proteins
194 ordinarily targeted to the apicoplast become stranded in small vesicles.[16] We confirmed
195 apicoplast loss in doxycycline and IPP-treated parasites by using microscopy to verify disrupted
196 apicoplast targeting of the nuclear-encoded ALAD enzyme (Figure 2d and Figure 2- figure
197 supplement 5), PCR to confirm loss of the small apicoplast genome (Figure 2- figure supplement
198 6), and western blot to visualize disruption of post-translational processing of ALAD (Figure 2-
199 figure supplement 7). Despite apicoplast disruption, these parasites retained their capacity for
200 heme biosynthesis (Figure 2a) and remained fully photosensitive in ALA (Figure 2e). Together
201 with the gene disruption results above, these observations strongly suggested that parasite-
202 infected erythrocytes have a parallel biosynthetic pathway that bypasses functional disruption of
203 the parasite enzymes targeted to the apicoplast and cytoplasm.
204
205 **Erythrocytes retain vestigial heme biosynthesis enzymes with latent activity stimulated by**
206 **ALA.** The heme biosynthesis pathway in human cells is distributed between mitochondria and

207 the cytoplasm, with four cytosolic enzymes that correspond to the four apicoplast-targeted
208 enzymes in *Plasmodium* parasites.[4,6,17] During human erythropoiesis, precursor reticulocytes
209 carry out prolific heme biosynthesis, but this activity is absent in mature erythrocytes due to loss
210 of mitochondria and their constituent heme biosynthesis enzymes, including ALA synthase and
211 ferrochelatase.[17] Proteomic studies have confirmed that mature erythrocytes retain the cytosolic
212 enzymes (ALAD, PBGD, UROS, and UROD),[18,19] but this vestigial pathway is ordinarily
213 quiescent due to the lack of ALA synthesis or uptake in erythrocytes. We hypothesized that
214 exogenous ALA taken up by parasite-infected erythrocytes might stimulate the latent activity of
215 these cytosolic human enzymes, resulting in biosynthetic flux through this truncated host
216 pathway and production of downstream tetrapyrrole intermediates that could be taken up by the
217 parasite via hemoglobin import or other mechanisms and converted into heme within the parasite
218 mitochondrion.

219 The cytosolic human enzymes remaining in the mature erythrocyte would be expected to
220 produce coproporphyrinogen III (CPP) from ALA. Our observation that disruption of the
221 parasite CPO had no effect on conversion of ALA into heme by intraerythrocytic parasites
222 suggests that a soluble fraction of human CPO, which is thought to be predominantly targeted to
223 the mitochondrial intermembrane space (IMS),[6,17] persists in the erythrocyte cytoplasm after
224 maturation of precursor reticulocytes and mitochondrial loss. Indeed, other mitochondrial IMS
225 proteins, such as cytochrome c, are known to partition into the cytoplasm under certain
226 conditions.[20,21] CPO catalyzes production of protoporphyrinogen IX, which in the oxygen-rich
227 environment of erythrocytes can spontaneously oxidize to form protoporphyrin IX.[22]

228 In support of this model, we noted that red porphyrin fluorescence in ALA-treated
229 infected erythrocytes was not limited to the parasite but was detectable throughout the

erythrocyte cytoplasm (Figure 1b), as expected for host enzyme activity and production of PPIX in this compartment. To directly test the model that enzymes remaining in the erythrocyte cytoplasm could catalyze PPIX biosynthesis from ALA, we permeabilized uninfected erythrocytes using the detergent saponin, clarified lysates by centrifugation followed by sterile filtration, and then used LC-MS/MS to monitor heme and porphyrin biosynthesis from 5-[$^{13}C_4$]-ALA added to the filtered lysate supernatant. We detected formation of ^{13}C-labelled PPIX and CPP but not heme, and this biosynthetic activity was fully blocked by succinylacetone (Figure 3a). These observations provide direct support for our model that erythrocytes retain a vestigial and partial biosynthesis pathway capable of converting exogenous ALA into PPIX but unable to convert PPIX to heme due to lack of mitochondria and ferrochelatase.

ALA uptake by erythrocytes requires new permeability pathways established by *Plasmodium* infection. In contrast to parasite-infected erythrocytes, uninfected erythrocytes showed no detectable porphyrin fluorescence in the presence of ALA (Figure 3b), consistent with reports that the erythrocyte membrane has a low permeability to amino acids.[23-25] Electroporation of uninfected erythrocytes in the presence of ALA, however, resulted in robust intracellular porphyrin fluorescence (Figure 3b), supporting our model that host enzymes have latent biosynthetic activity that requires a mechanism for ALA uptake across the normally impermeable erythrocyte membrane.

Upon invasion, *Plasmodium* parasites export hundreds of effector proteins into host erythrocytes. These proteins dramatically alter the architecture of the infected erythrocyte and establish new permeability pathways (NPP) that enhance host cell uptake of amino acids and

252 other nutrients from host serum.[26] We hypothesized that selective uptake of ALA by parasite-
253 infected erythrocytes was mediated by NPP mechanisms.

254 To test this model, we utilized a recently published parasite line in which the export of
255 parasite proteins into host erythrocytes, including establishment of nutrient permeability
256 pathways, can be conditionally regulated with the synthetic small-molecule ligand trimethoprim
257 (TMP).[27] In these parasites, protein export and NPP mechanisms are functional in the presence of
258 TMP but are blocked in its absence. We maintained or washed out TMP from a synchronized
259 culture of late schizonts, allowed parasites to rupture and reinvade new erythrocytes, and then
260 incubated both sets of parasites in ALA for 8 hours. Whereas TMP-treated parasites with normal
261 protein export and permeability displayed robust PPIX fluorescence indistinguishable from that
262 of wild-type parasites, parasites incubated without TMP showed no detectable PPIX fluorescence
263 (Figure 3c). We observed similar results in wild-type parasites using the small-molecule drug
264 furosemide, which blocks parasite-derived NPP mechanisms directly (Figure 3- figure
265 supplement 1).[28] We conclude that ALA is selectively taken up by infected erythrocytes via
266 parasite-dependent nutrient acquisition pathways and metabolized to PPIX by vestigial host
267 enzymes within the erythrocyte cytoplasm (Figure 4).
268
269 ***Plasmodium*-encoded heme biosynthesis pathway has no detectable activity during blood-**
270 **stage infection.** Our observation that disruption of the parasite-encoded PBGD and CPO does
271 not affect biosynthetic production of heme and PPIX from ALA suggests that host enzyme
272 activity in the erythrocyte cytoplasm provides the dominant contribution to PPIX biosynthesis in
273 ALA-treated intraerythrocytic parasites. To dissect these parallel pathways and test whether the
274 parasite pathway alone, in the absence of host enzymes, can support heme biosynthesis from

ALA, we fractionated parasite-infected erythrocytes using saponin to selectively permeabilize host cell membranes while leaving parasite membranes intact (Figure 5a). Under these conditions, soluble erythrocyte proteins can be washed away to leave the intact live parasite natively embedded within the resulting erythrocyte ghost (Figure 5b,c). Parasites treated in this fashion remain metabolically active for 5-6 hours or longer, retain a membrane potential, accumulate fluorescent dyes such a mitotracker red (Figure 5b,c), and carry out DNA synthesis.[29,30] After saponin treatment and washout, we placed parasites back into culture medium containing ^{13}C-ALA and incubated them overnight before extracting them for analysis by LC-MS/MS. We failed to detect biosynthesis of heme, PPIX, or CPP in fractionated asexual and sexual blood-stage parasites (Figure 5d), suggesting that the apicoplast-localized portion of the parasite heme biosynthesis pathway is largely or completely inactive during blood-stage infection.

To test this conclusion within undisrupted parasites, we created a transgenic parasite line expressing an apicoplast-targeted version of the uroporphyrinogen III methyltransferase (cobA) protein from *Propionibacterium freudenreichii* to serve as a biosensor of heme biosynthesis pathway activity within the parasite apicoplast. The cobA protein catalyzes conversion of the heme biosynthesis intermediate uroporphyrinogen III into the red fluorescent products sirohydrochlorin and trimethylpyrrocorphin (Figure 6a) and has been shown to function when heterologously expressed in bacteria (Figure 6b), yeast, and mammalian cells.[31,32] We targeted a cobA-GFP fusion protein to the apicoplast in ALA-treated parasites (Figure 6c) but were unable to detect any red fluorescence in this organelle indicative of cobA-mediated conversion of uroporphyrinogen III to the fluorescent products, suggesting that parasite enzymes targeted to this organelle are inactive in both asexual and sexual blood stages (Figure 6d,e). We also noted

298 that growth of ΔFC parasites,[10] which would be expected to accumulate PPIX during native
299 pathway activity (Figure 1a), was insensitive to light in the absence of ALA (Figure 6- figure
300 supplement 1). These observations suggest that heme biosynthesis in blood-stage *P. falciparum*
301 parasites is only operative when exogenous ALA is present to stimulate PPIX production by
302 remnant host enzymes in the erythrocyte cytoplasm, with subsequent PPIX uptake and
303 conversion to heme by ferrochelatase in the parasite mitochondrion (Figure 4).
304
305 **Development of chemiluminescence-based photodynamic therapy for treatment of blood-**
306 **stage malaria.** Our results and those of prior studies suggested that stimulation of heme
307 biosynthesis might be exploited for antimalarial photodynamic therapy (PDT). Conventional
308 PDT requires an external light source to photoactivate and kill ALA-stimulated cells.[13,33,34]
309 While such approaches can successfully target localized shallow-tissue tumors,[13,34] they are
310 impractical for treating malaria due to the dispersed nature of blood-stage infection, the
311 sequestration of mature *P. falciparum* parasites along the vascular endothelium, and the
312 requirement to illuminate every infected erythrocyte.
313 To bypass the need for external light, chemiluminescence has been proposed as an
314 alternative means to photoactivate the cytotoxicity of PPIX in ALA-stimulated cells. Trial
315 studies in cancer cell lines have shown modest success using the small molecule luminol,[35,36]
316 whose iron-activated chemiluminescence[37] overlaps the absorbance spectrum of PPIX (Figure 7-
317 figure supplement 1). Cancer cells tightly sequester iron, which may limit luminol activation in
318 these environments. *Plasmodium* parasites, however, expose abundant iron during large-scale
319 digestion of erythrocyte hemoglobin and liberation of heme. We therefore hypothesized that

320 intraerythrocytic parasites might show heightened susceptibility to chemiluminescence-based
321 photodynamic therapy (CL-PDT) (Figure 6a).

322 To test the efficacy of a CL-PDT strategy for targeting blood-stage *P. falciparum*, we
323 incubated intraerythrocytic parasites with twice-daily media changes in combinatorial treatments
324 of ALA, luminol, and 4-iodophenol, a small-molecule that has been shown to enhance the
325 intensity and duration of luminol chemiluminescence.[38] Parasites treated with optimized
326 concentrations each compound in single or double combination showed little effect on parasite
327 growth (Figure 7- figure supplement 2). The combination of all three compounds, however,
328 potently inhibited parasite growth (Figure 6b), and microscopic examination by blood-smear
329 revealed widespread parasite death (Figure 7- figure supplement 3). The growth effects of this
330 combination could be fully rescued by succinylacetone (Figure 6b), supporting a photodynamic
331 mechanism requiring PPIX biosynthesis from ALA and and enhanced chemiluminescence by
332 luminol.

333 The development of parasite resistance to frontline antimalarial drugs continues to
334 hamper malaria treatment and eradication efforts worldwide. To test whether a CL-PDT
335 mechanism remains effective against parasites with diverse resistance to distinct drugs, we
336 turned to studies with Dd2 parasites, which have multidrug resistance to antifolate and quinolone
337 antibiotics,[39] and a clinical isolate containing a kelch-13 protein mutation that confers
338 artemisinin tolerance.[2] In both parasite lines, combination treatment with ALA, luminol, and 4-
339 iodophenol potently ablated parasite growth (Figure 7- figure supplement 4).

340 Artemesinin and its derivatives are current frontline drugs used for treatment of malaria,
341 usually in combination with a partner drug. Artemisinin, whose endoperoxide moiety is
342 reductively cleaved by intracellular iron to generate reactive oxygen radicals,[40] has been shown

to potently stimulate luminol chemiluminescence *in vitro*,[41] suggesting the possibility of combining CL-PDT with artemisinin for antimalarial treatment. To test the efficacy of an artemisinin-enhanced CL-PDT strategy, we incubated 3D7 parasites with twice-daily media changes in ALA, luminol, and sub-therapeutic doses (500 pM, 10% of EC_{50}, Figure 7- figure supplement 5) of dihydroartemisinin (DHA). Single and double combinations had little effect (Figure 7- figure supplement 6), but all three compounds together potently ablated parasite growth, and growth inhibition could be fully rescued with succinylacetone (Figure 6c).

Discussion

Malaria parasites, like nearly all other organisms, have a metabolic requirement for heme.[5-7] Despite access to abundant host heme during intraerythrocytic infection, parasites retain a complete heme biosynthesis pathway that was regarded for two decades as essential and a potential drug target.[9] Our work and recent studies have now successfully disrupted four of the eight pathway enzymes, providing firm evidence that *de novo* heme synthesis is dispensable during blood-stage infection. These data strongly suggest that parasites have mechanisms to scavenge host heme to meet metabolic needs and clarify that heme biosynthesis is not a viable target for classical drug inhibition.[10,11]

Our results further suggest that the parasite pathway is not active during intraerythrocytic infection. This inactivity may reflect the low availability of the succinyl-CoA precursor due to limited TCA cycle flux[42] and additional regulatory mechanisms, such as feedback inhibition by host heme or active site inhibition by endogenous metabolites,[43] that suppress the activity of apicoplast-targeted enzymes during blood-stage parasite development. The functional quiescence of this specific biosynthetic pathway, despite expression of the constituent enzymes, may reflect

366 a general survival strategy and adaptation by parasites to closely match metabolic requirements
367 with nutritional availability within specific host environments, such as previously described for
368 parasite acquisition of fatty acids.[44] Indeed, prior studies suggest that the parasite heme synthesis
369 pathway is required for development within the mosquito and human liver,[10,11] host
370 environments with lower heme availability compared to erythrocytes and in which parasite heme
371 requirements appear to be elevated due to enhanced reliance on mitochondrial electron transport
372 for ATP synthesis.[5,6,45] A prior study also reported that blood-stage *P. falciparum* parasites adopt
373 distinct physiological states *in vivo*, including a state with heightened oxidative metabolism and
374 mitochondrial activity that may arise during host starvation.[46] It remains a future challenge to test
375 whether heme biosynthesis by the parasite-encoded pathway can be stimulated by host
376 nutritional status during intraerythrocytic infection.

377 Despite the dispensable nature and apparent inactivity of the parasite-encoded heme
378 biosynthesis pathway, infected erythrocytes retain a paradoxical ability to synthesize heme from
379 exogenous ALA. This biosynthetic activity requires the *Plasmodium* ferrochelatase but not the
380 upstream enzymes in the parasite pathway. Indeed, knock-out of the *Plasmodium* FC prevented
381 conversion of PPIX to heme,[10] but our disruption of the parasite PBGD and CPO genes, as well
382 as the entire apicoplast organelle, had no effect on ALA-stimulated heme synthesis (Figure 2).
383 Our work resolves this paradox by identifying a latent contribution to heme biosynthesis in
384 parasite-infected erythrocytes from vestigial host enzymes remaining in the erythrocyte
385 cytoplasm. Since erythrocytes lack mitochondria, they are missing the initial and terminal
386 pathway enzymes, cannot synthesize ALA, and thus retain only a truncated and normally
387 inactive heme synthesis pathway. Analytical studies have reported that human serum contains
388 0.1-0.2 μM ALA,[47] but the low permeability of the erythrocyte membrane to ALA means that

389 extracellular ALA is largely inaccessible to vestigial host enzymes within uninfected
390 erythrocytes.

391 Our study clarifies that NPP mechanisms of parasite-infected red blood cells enable
392 efficient uptake of exogenous ALA, which can be metabolized by vestigial human enzymes
393 within the oxygen-rich erythrocyte cytoplasm to produce PPIX that can be converted to heme by
394 FC within the parasite mitochondrion (Fig. 4). Thus, the 0.2 μM ALA natively present in human
395 serum may be sufficient to stimulate low-level heme biosynthesis within parasites *in vivo*.
396 Indeed, we detect ^{13}C-labeled PPIX in parasites grown in 1 μM 5-[$^{13}C_4$]-ALA *in vitro* (Figure 4-
397 figure supplementary 1), supporting a model that serum ALA stimulates heme biosynthesis
398 during malaria infection *in vivo*. Such activity, however, is not required to support blood-stage
399 parasite growth. We note that prior work suggested a role for remnant host enzymes in heme
400 biosynthesis by malaria parasites, but this proposal differed by positing that human enzymes
401 such as ALAD were somehow imported and active within the parasite cytoplasm.[48]

402 The ability to photosensitize parasites with exogenous ALA and then kill them with light
403 introduces exciting possibilities for developing new photodynamic treatment strategies,
404 exemplifies how deep understanding of fundamental parasite metabolism can be leveraged for
405 designing novel therapies, and highlights that non-essential pathways can still serve as
406 therapeutic targets. We have shown that luminol-based chemiluminescence, when stimulated by
407 combinatorial delivery of low-dose 4-iodophenol or artemisinin, can circumvent the
408 conventional PDT requirement for external light and potently ablate parasite growth (Figure 6).
409 We note that ALA, luminol, and DHA have excellent toxicity profiles, favorable
410 pharmacokinetic properties, and have each been used clinically.[34,49-52] These results suggest the
411 possibility of including ALA and luminol with therapeutic doses of artemisinin (or its clinical

derivatives) as a novel form of artemisinin combination therapy for treating malaria. Multidrug-resistant parasites remain susceptible to this photodynamic strategy, which relies on host enzyme activity outside the genetic control of parasites and thus is refractory to development of resistance-conferring mutations. This strategy may also be effective against other intraerythrocytic parasites, such as *Babesia*. As for any new therapy suggested by *in vitro* studies, additional *in vivo* experiments will be required to optimize treatment regimens for our proposed therapy and to confirm efficacy and safety.

Finally, we note that this strategy of using artemisinin to stimulate intracellular light emission by luminol for ALA-based photodynamic therapy may be applicable to treating deep-tissue cancers, for which poor accessibility to external light also limits current PDT approaches in development for cancer therapy.[13] Artemisinin has shown promising anti-cancer properties on its own,[53] and thus its combination with ALA and luminol may provide potent synergy for cancer chemotherapy.

Materials and Methods

Materials. All reagents were of the highest purity commercially available. Succinylacetone, 5-aminolevulinic acid, 4-iodophenol, trimethoprim, furosemide, saponin, isopentenyl pyrophosphate, doxycycline, luminol, and dihydroartemisinin were purchased from Sigma. 5-[$^{13}C_4$]-aminolevulinic acid was purchased from Cambridge Isotope Laboratories, Inc.

Microscopy. Images of live or fixed parasites were acquired on an Axio Imager.M1 epifluorescence microscope (Carl Zeiss Microimaging, Inc.) equipped with a Hamamatsu ORCA-ER digital CCD camera and running Axiovision 4.8 software, as described previously.[54]

Live parasite nuclei were stained with 5 μM Hoechst 3342 added immediately prior to image acquisition. For photodynamic imaging studies, parasites were cultured in 200-500 μM ALA in the absence or presence of 50 μM succinylacetone for 6-12 hours prior to visualization. Hemozoin movement in parasite digestive vacuoles was imaged by acquiring 10-20 sequential frames at 1 second intervals on the bright-field channel. Images were cropped and superimposed in Adobe Photoshop and exported as movie files with a 0.1 second frame delay. Immunofluorescence images were acquired by fixing and staining parasites as previously described.[55,56] Electron microscopy images of parasites subjected to light or 500 μM ALA + light were obtained as previously described.[27] Uninfected erythrocytes were washed and resuspended in 1X cytomix containing 500 μM ALA, electroporated in a manner identical to parasite transfections (see below), washed in PBS, incubated overnight at 37˚ C, and imaged as described above for live parasites. Images acquired on different channels for common samples were processed with identical brightness and contrast settings.

Parasite growth analysis. Parasite growth was monitored by diluting asynchronous parasites to 0.5% parasitemia and allowing culture expansion with daily or twice daily media changes. Parasitemia was measured daily by diluting 10 μl of each resuspended culture in 200 μl acridine orange (1.5 μg/ml) and analyzing by flow cytometry, as previously described.[57] To assess the light sensitivity of ALA-treated parasites, asynchronous parasites were cultured in 200μM ALA in the absence or presence of 50 μM succinylacetone and subjected to 2 minute daily exposures to broad wavelength white light on an overhead projector. Daily parasitemia measurements were plotted as a function of time and fit to an exponential growth equation using GraphPad Prism 5.0.

For chemiluminescence experiments, asynchronous parasites were diluted to 0.5% parasitemia and incubated ±100 μM ALA and ±50 μM succinylacetone for 8 hours. After 8 hours, parasite media was changed to also include 750 μM luminol, 50 μM 4-iodophenol, and 0.5 nM dihydroartemisinin in the indicated combinations. Parasite cultures were allowed to expand over 5 days, with twice-daily (7 am and 4 pm) media changes in the indicated combinations. Parasitemia was measured daily on replicate samples, as indicated above. Experiments were performed using 3D7 (drug sensitive) parasites, Dd2 (multidrug resistant) parasites[39], and a clinical isolate[2] (MRA-1241) bearing the I543T mutation in the Kelch-13 gene locus responsible for artemisinin tolerance. Exposure of parasite cultures to ambient light was minimized by changing media within darkened TC hoods and covering parasite culture dishes during brief (5-10 sec.) transits to and from incubators. The effect of 100 μM ALA on parasite growth varied slightly between experiments, possibly due to differences between distinct batches of donated erythrocytes.

For IC_{50} determinations, asynchronous parasites were diluted to 1% parasitemia and incubated with variable drug concentrations for 48 hours without media change. After 48 hours, parasitemia was determined in duplicate samples for each drug concentration, normalized to the parasitemia in the absence of drug, plotted as a function of the log of the drug concentration, and fit to a sigmoidal growth inhibition curve using GraphPad Prism 5.0.

Parasite strains, culture, genetic modification, and transgene expression. Parasite culture and transfection were performed in RPMI supplemented with Albumax, as previously described.[54] Cloning was performed using either restriction endonuclease digestion and ligation or the In-Fusion system (Clontech).

For episomal expression of *P. falciparum* ALA dehydratase (PF3D7_1440300) and coproporphyrinogen III oxidase (CPO, PF3D7_1142400) fused to a C-terminal GFP tag (ALAD-GFP and CPO-GFP), cDNA inserts encoding the complete ALAD and CPO genes (exons only) were RT-PCR-amplified from total parasite RNA using the Superscript III system (Life Technologies) and primers CACTATAGAACTCGAGATGTTAAAATCAGATGTA GTGCTTTTATTGTATATAC and CTGCACCTGGCCTAGGTAGAGTTAATTCTATATT AAAATTATTATTTGAATTATCATC (ALAD) or ACGATTTTTTCTCGAGATGAAA GATGAGATAGCTCCTAATGAATATTTTAGAAATTTATG and CTGCACCTGGCCT AGGGTAGTCCACCCACTTTTTGGGATAC (CPO), digested with XhoI/AvrII, and ligated into the XhoI/AvrII sites of a digested pTEOE vector that was identical to a previously described pTyEOE vector[27] except that the pTEOE plasmid contained human DHFR in place of yeast DHOD as the positive selection marker. Plasmid-based expression of the ALAD-GFP fusion was driven by the HSP86 promoter. This plasmid (50 μg) was co-transfected into 3D7 parasites along with plasmid pHTH (10 μg) for transient expression of the *piggyback* transposase that mediates integration of the pTEOE plasmid into the parasite genome.[58] Parasites were selected with 5 nM WR99210.

For episomal expression of *Propionibacterium freudenreichii* (*shermanii*) uroporphyrinogen III methyltransferase (cobA) (Genbank: CBL55989.1) targeted to the parasite apicoplast, the cobA gene was PCR-amplified from plasmid pISA417[31] using the primers ACGATTTTTTCTCGAGATGACCACCACACTGTTGCCCGGCACTGTC and CTGCACCT GGCCTAGGGTGGTCGCTGGGCGCGCGATGG, digested with XhoI/AvrII, and ligated into the XhoI/AvrII-cut pTEOE vector described above. An insert encoding the *P. falciparum* acyl carrier protein (ACP) leader sequence (residues 1-60) with 5'- and 3'- XhoI sites, previously

503 PCR-amplified from parasite cDNA,[54] was digested with XhoI and ligated into the XhoI-cut
504 cobA/pTEOE vector to generate an in-frame ACP_L-cobA-GFP fusion gene. This plasmid was co-
505 transfected with pHTH into 3D7 parasites as described above.
506 For disruption of the *P. falciparum* genes encoding PBGD (PF3D7_1209600) and CPO
507 (PF3D7_1142400), primer pairs (PBGD: CACTATAGAACTCGAGGATCATAATAA
508 TGATACATTATGTACTATTGGGACATCGTCC and CTGCACCTGGCCTAGGAA
509 CTGCTATAATGCCTTGACCTAAGGCAGGATAAATCAGG; CPO: CACTATAG
510 AACTCGAGTTTTTTCAAATATTTATAAAAACAGGAAAAAAGAAGAAAAAATA and
511 CTGCACCTGGCCTAGGATAACATTTACAATCCTTATTATTATTATTATTATTGTTG
512 ATGG) were used to PCR-amplify 360 bp and 471 bp sequences from the middle of the 1.3 kb
513 PBGD and 1.6 kb CPO genes, respectively. These inserts were cloned by In-Fusion into the
514 XhoI/AvrII sites of the pPM2GT vector,[59] which encodes a C-terminal GFP tag after the AvrII
515 site and also contains a human DHFR marker for positive selection with 5 nM WR99210. This
516 vector was further modified to introduce a 2A peptide sequence[60] followed by the yeast
517 dihydroorotate dehydrogenase (yDHOD) sequence[61], after the 3' end of the GFP cassette, to
518 enable positive selection for integration with the parasite DHOD inhibitor, DSM1. The yDHOD
519 marker, however, was not used for selection in this study, and use of this GFP-2A-
520 yDHPD/PM2GT vector for positive selection of plasmid integration into the genome will be
521 described elsewhere. Plasmids (50 μg) were transfected into 3D7 parasites by electroporation.
522 Parasites were subjected to three rounds of positive selection with 5 nM WR99210. After the
523 first and second selections, cultures were maintained for three weeks in the absence of drug
524 pressure prior to the subsequent round of positive selection. After the third round of positive
525 selection, parasites were cloned by limiting dilution. Clonal parasites that had integrated the

plasmid at the desired locus to disrupt the target genes by single cross-over homologous recombination were verified by PCR and Southern blot, as previously described,[59] and retained for further analysis.

To introduce a C-terminal GFP tag into the endogenous locus of the *P. falciparum* PBGD gene (PF3D7_1209600), primer pairs CACTATAGAACTCGAGGATCATAATAA TGATACATTATGTACTATTGGGACATCGTCC and CTGCACCTGGCCTAGGTTTATTA TTTAAAAGGTGCAATTCAGCCTCCGCTTTTATTTTG were used to PCR-amplify the complete PBGD coding sequence. This insert was cloned by In-Fusion into the 2A-yDHOD/PM2GT vector described above and transfected into 3D7 parasites by electroporation as above. Stable integration was achieved after three rounds of positive selection in WR99210, and clones were isolated by limiting dilution and verified by PCR and southern blot.

ΔFC D10 parasites, described in a prior study[10], were obtained from Akhil Vaidya (Drexel University) and were cultured as described above, including two-minute daily exposures to broad-wavelength white light using an overhead projector light box.

For apicoplast disruption experiments, parasites were cultured in 1 μM doxycycline and 200 μM IPP for 7-21 days.[16] After 7 days, genomic DNA was harvested and analyzed by PCR for the nuclear-encoded acyl carrier protein (ACP) gene (primers ATGAAGATCTTATTACTTTGTATAATTTTTC and TTTTAAAGAGCTAGATGGGTTTTT ATTTTTTATC) and apicoplast-encoded rps8 (primers ATGATTATTAAATTTTTAAATAATG and TTACAAAATATAAAATAATAAAATACC) and ORF91 (primers ATGACTTT ATATTTAAATAAAAATTT and TTACATATTTTTTTTATTGAAGAACG) genes to confirm selective loss of the apicoplast genome.

549 **Gametocyte Induction and Culturing.** 3D7 ΔPM1 (plasmepsin 1) parasites[62] and 3D7 parasites
550 expressing ACP_{leader}-cobA-GFP from a TEOE plasmid (described above) were synchronized
551 using 5% sorbitol and cultured using gentamycin-free media. Gametocytogenesis was stress-
552 induced in mid-trophozoite parasites (5-7% parasitemia) by increasing hematocrit to 4% (by
553 removing half of the culture medium volume) for 12 hours. Parasites were maintained in culture
554 for 4-6 days, at which point mostly stage III-IV gametocytes were visible. ACP_{leader}-cobA-GFP
555 gametocytes were incubated overnight in the presence or absence of 500 μM ALA and imaged
556 by live parasite microscopy as described above. For ^{13}C-ALA labeling experiments, gametocytes
557 were passaged over a magnetic column to remove uninfected erythrocytes and concentrate the
558 gametocyte-infected cells, lysed in 0.02% saponin (0.2-μM filtered), placed back into culture
559 medium containing 200 μM 5-[$^{13}C_4$]-ALA, and incubated overnight at 37˚ C. Parasites were then
560 isolated by centrifugation, extracted, and analyzed by tandem mass spectroscopy as described
561 below.
562
563 **Analysis of heme biosynthesis by ^{13}C-labeling and liquid chromatography-tandem mass**
564 **spectrometry (LC-MS/MS).** Parasites were cultured in 200 μM 5-[$^{13}C_4$]-ALA for 12-24 hours,
565 harvested by centrifugation, lysed in 0.05% cold saponin, washed in PBS, and extracted with
566 DMSO. Deuteroporphyrin was added as an internal standard, and extracts were analyzed for ^{13}C-
567 labeled heme, PPIX, and CPPIII using a previously published LC-MS/MS assay.[10] Detection of
568 coproporphyrin III (CPPIII) serves as a biomarker for detecting coproporphyrinogen III, which is
569 rapidly oxidized to CPPIII upon exposure to air during cell lysis and extraction.[22]
570

571 **Fractionation of parasite-infected erythrocytes.** To assess whether parasites could synthesize
572 heme from ALA in the absence of host enzymes in the erythrocyte cytoplasm, parasite-infected
573 red blood cells were lysed with 0.05% saponin (0.2 μM filtered), spun briefly (3 min., 850 x g) to
574 pellet, washed in PBS, and resupended in 12 ml of RPMI/albumax growth media supplemented
575 with 200 μM 5-[$^{13}C_4$]-ALA. Parasites were incubated over-night at 37˚ C, harvested by
576 centrifugation, and extracted and analyzed by tandem mass spectrometry as described above.
577
578 **Preparation of lysates from uninfected erythrocytes.** To assess the heme biosynthesis capacity
579 of the erythrocyte cytoplasm, 500 μl packed red blood cells (described previously[54]) were lysed
580 in 20 ml of 0.04% saponin/PBS (0.2 μM filtered) and centrifuged at 25,000 x g for 60 minutes to
581 pellet unlysed cells and any organelles. The superficial 15 ml of the lysate supernatant was
582 removed and 0.2 μM filtered, supplemented with 200 μM 5-[$^{13}C_4$]-ALA in the absence or
583 presence of 50 μM succinylacetone, incubated overnight at 37˚ C, and analyzed by tandem mass
584 spectrometry as described above.
585
586 **Chemical block of parasite nutrient uptake pathways.** The 3D7 parasite line expressing the
587 endogenous HSP101 from its genomic locus and bearing a C-terminal *E. coli* DHFR degradation
588 domain (DDD) fusion tag was previously published.[27] To test whether ALA-uptake by parasite-
589 infected erythrocytes depends on parasite-established nutrient acquisition pathways in the host
590 cell membrane, we split a synchronous culture of HSP101-DDD into two populations of late
591 schizonts (purified over a magnetic column) and washed out trimethoprim (TMP) from one of
592 the two cultures. Both cultures (±TMP) were permitted to lyse and reinvade fresh erythrocytes
593 overnight. The following morning, parasites were placed in 200 μM ALA as early rings,

incubated for 8 hours at 37˚ C, and imaged by live parasite microscopy as described above. Alternatively, asynchronous wild-type 3D7 parasites were incubated in the absence or presence of 100 μM furosemide for one hour to block nutrient acquisition pathways, followed by addition of 500 μM ALA and further incubation for eight hours. Parasites were then imaged by live parasite microscopy as described above.

Antibodies and Live Cell Stains. The following antibodies were used for immunofluorescence (IFM) and western blot (WB) analysis at the indicated dilutions: goat anti-GFP (Abcam 5450) (IFM 1:500, WB 1:1000), rabbit anti-ACP[56,63] (IFM: 1:500), Alexa Fluor 488-conjugated chicken anti-goat (IFM: 1:500), Alexa Fluor 555-conjugated donkey anti-rabbit (IFM: 1:500), donkey anti-goat- IRDye 800 (Licor Biosciences) (WB: 1:10,000). Mitotracker Red was used at 50 nM final concentration and was added to parasite cultures 30 minutes prior to harvest and analysis.

Absorbance and Luminescence Spectroscopy. Fluorescence excitation and emission spectra of pure PPIX in aqueous solution (excitation 400 nm, emission 620 nm) and of clarified lysates of *E. coli* bacteria expressing cobA (excitation 360 nm, emission 600 nm) and chemiluminescence spectra of luminol were obtained on a Cary Eclipse fluorescence spectrophotometer (Varian, Inc.) in either fluorescence or luminescence mode using 10-nm slit widths and a PMT detector voltage setting of 600. Luminol solutions contained 25 mM luminol in 100 mM NaOH (aq) to which 0.1% (w/v) ammonium persulfate (aq) was added to stimulate light emission.

Imaging hemozoin dynamics in parasite digestive vacuole. Time-lapse bright field images of parasites were acquired with 1 sec. delays, composed into movie files using Adobe Photoshop, and played back with 0.1 sec. delays between frames. Bright field images were acquired before and after 4 sec. image acquisitions with the Zeiss filter sets 38 (excitation 450-490 nm) and 43 HE (excitation 537-562 nm).

Homology Models. Homology models of PBGD and CPO were generated using the Swiss-Model interface on the Expasy website (http://swissmodel.expasy.org). The template structures for modeling were human PBGD (PBD: 3EQ1) and human CPO (PDB: 2AEX).

Acknowledgements

We thank W. Beatty for assistance with electron microscopy, A. Oksman for assistance with gametocyte culturing, A. Vaidya and H. Ke for providing ΔFC parasites, and C. Roessner for the pISA417 plasmid encoding the cobA gene. We thank J. Phillips, D. Winge, T. Hasan, B. Striepen, A. Vaidya, I. Hamza, and members of the Goldberg lab for helpful discussions. This work was supported by National Institutes of Health grants R21 AI110712-01 (to D.E.G.) and R01 DK099534 (to J.P.H.) and by a Burroughs Wellcome Fund Career Award for Medical Scientists (to J.P.H.) and Career Award at the Scientific Interface (to. P.A.S.).

References

1 WHO. World Malaria Report 2014. (Switzerland).

2 Ariey, F. *et al.* A molecular marker of artemisinin-resistant Plasmodium falciparum malaria. *Nature* **505**, 50-55 (2014).

3 Dondorp, A.M. *et al.* Artemisinin Resistance in Plasmodium falciparum Malaria. *New Engl. J. Med.* **361**, 455-467 (2009).
4 Ponka, P. Cell biology of heme. *Am. J. Med. Sci.* **318**, 241-256 (1999).
5 Sigala, P.A. & Goldberg, D.E. The peculiarities and paradoxes of Plasmodium heme metabolism. *Annu. Rev. Microbiol.* **68**, 259-278 (2014).
6 van Dooren, G.G., Kennedy, A.T. & McFadden, G.I. The use and abuse of heme in apicomplexan parasites. *Antioxid. Redox Signal.* **17**, 634-656 (2012).
7 Painter, H.J., Morrisey, J.M., Mather, M.W. & Vaidya, A.B. Specific role of mitochondrial electron transport in blood-stage *Plasmodium falciparum*. *Nature* **446**, 88-91 (2007).
8 Gardner, M.J. *et al.* Genome sequence of the human malaria parasite *Plasmodium falciparum*. *Nature* **419**, 498-511 (2002).
9 Surolia, N. & Padmanaban, G. De novo biosynthesis of heme offers a new chemotherapeutic target in the human malarial parasite. *Biochem. Biophys. Res. Commun.* **187**, 744-750 (1992).
10 Ke, H. *et al.* The heme biosynthesis pathway is essential for Plasmodium falciparum development in mosquito stage but not in blood stages. *J. Biol. Chem.* **289**, 34827-34837 (2014).
11 Nagaraj, V.A. *et al.* Malaria parasite-synthesized heme is essential in the mosquito and liver stages and complements host heme in the blood stages of infection. *PLoS Pathog.* **9**, e1003522 (2013).
12 Kennedy, J.C., Pottier, R.H. & Pross, D.C. Photodynamic Therapy with Endogenous Protoporphyrin .9. Basic Principles and Present Clinical-Experience. *J. Photoch. Photobio. B* **6**, 143-148 (1990).
13 Celli, J.P. *et al.* Imaging and photodynamic therapy: mechanisms, monitoring, and optimization. *Chem. Rev.* **110**, 2795-2838 (2010).
14 Smith, T.G. & Kain, K.C. Inactivation of Plasmodium falciparum by photodynamic excitation of heme-cycle intermediates derived from delta-aminolevulinic acid. *J. Infect. Dis.* **190**, 184-191 (2004).
15 Dahl, E.L. *et al.* Tetracyclines specifically target the apicoplast of the malaria parasite Plasmodium falciparum. *Antimicrob. Agents Chemother.* **50**, 3124-3131 (2006).
16 Yeh, E. & DeRisi, J.L. Chemical rescue of malaria parasites lacking an apicoplast defines organelle function in blood-stage Plasmodium falciparum. *PLoS Biol.* **9**, e1001138 (2011).
17 Ponka, P. Tissue-specific regulation of iron metabolism and heme synthesis: distinct control mechanisms in erythroid cells. *Blood* **89**, 1-25 (1997).
18 Pasini, E.M. *et al.* In-depth analysis of the membrane and cytosolic proteome of red blood cells. *Blood* **108**, 791-801 (2006).
19 D'alessandro, A., Righetti, P.G. & Zoha, L. The Red Blood Cell Proteome and Interactome: An Update. *J. Proteome Res.* **9**, 144-163 (2010).
20 Soltys, B.J. & Gupta, R.S. Mitochondrial proteins at unexpected cellular locations: Export of proteins from mitochondria from an evolutionary perspective. *Int. Rev. Cytol.* **194**, 133-196 (2000).
21 Liu, X.S., Kim, C.N., Yang, J., Jemmerson, R. & Wang, X.D. Induction of apoptotic program in cell-free extracts: Requirement for dATP and cytochrome c. *Cell* **86**, 147-157 (1996).

685 22 Wang, Y. *et al.* Direct assay of enzymes in heme biosynthesis for the detection of
686 porphyrias by tandem mass spectrometry. Uroporphyrinogen decarboxylase and
687 coproporphyrinogen III oxidase. *Anal. Chem.* **80**, 2599-2605 (2008).
688 23 Desai, S.A., Bezrukov, S.M. & Zimmerberg, J. A voltage-dependent channel involved in
689 nutrient uptake by red blood cells infected with the malaria parasite. *Nature* **406**, 1001-
690 1005 (2000).
691 24 Kirk, K., Horner, H.A., Elford, B.C., Ellory, J.C. & Newbold, C.I. Transport of Diverse
692 Substrates into Malaria-Infected Erythrocytes Via a Pathway Showing Functional-
693 Characteristics of a Chloride Channel. *J. Biol. Chem.* **269**, 3339-3347 (1994).
694 25 Ginsburg, H., Kutner, S., Krugliak, M. & Cabantchik, Z.I. Characterization of Permeation
695 Pathways Appearing in the Host Membrane of Plasmodium-Falciparum Infected Red
696 Blood-Cells. *Mol. Biochem. Parasitol.* **14**, 313-322 (1985).
697 26 Spillman, N.J., Beck, J.R. & Goldberg, D.E. Protein Export into Malaria Parasite-
698 Infected Erythrocytes: Mechanisms and Functional Consequences. *Annu. Rev. Biochem.*
699 (2015).
700 27 Beck, J.R., Muralidharan, V., Oksman, A. & Goldberg, D.E. PTEX component HSP101
701 mediates export of diverse malaria effectors into host erythrocytes. *Nature* **511**, 592-595
702 (2014).
703 28 Staines, H.M. *et al.* Furosemide analogues as potent inhibitors of the new permeability
704 pathways of Plasmodium falciparum-infected human erythrocytes. *Mol. Biochem.*
705 *Parasitol.* **133**, 315-318 (2004).
706 29 Cobbold, S.A., Martin, R.E. & Kirk, K. Methionine transport in the malaria parasite
707 Plasmodium falciparum. *Int. J. Parasitol.* **41**, 125-135 (2011).
708 30 Izumo, A., Tanabe, K. & Kato, M. A Method for Monitoring the Viability of Malaria
709 Parasites (Plasmodium-Yoelii) Freed from the Host Erythrocytes. *Trans. R. Soc. Trop.*
710 *Med. Hyg.* **81**, 264-267 (1987).
711 31 Sattler, I. *et al.* Cloning, sequencing, and expression of the uroporphyrinogen III
712 methyltransferase cobA gene of Propionibacterium freudenreichii (shermanii). *J.*
713 *Bacteriol.* **177**, 1564-1569 (1995).
714 32 Wildt, S. & Deuschle, U. cobA, a red fluorescent transcriptional reporter for Escherichia
715 coli, yeast, and mammalian cells. *Nat. Biotechnol.* **17**, 1175-1178 (1999).
716 33 Juzeniene, A., Peng, Q. & Moan, J. Milestones in the development of photodynamic
717 therapy and fluorescence diagnosis. *Photochem. Photobiol. Sci.* **6**, 1234-1245 (2007).
718 34 Wachowska, M. *et al.* Aminolevulinic Acid (ALA) as a Prodrug in Photodynamic
719 Therapy of Cancer. *Molecules* **16**, 4140-4164 (2011).
720 35 Chen, T.C., Huang, L., Liu, C.C., Chao, P.J. & Lin, F.H. Luminol as the light source for
721 in situ photodynamic therapy. *Process Biochem.* **47**, 1903-1908 (2012).
722 36 Laptev, R., Nisnevitch, M., Siboni, G., Malik, Z. & Firer, M.A. Intracellular
723 chemiluminescence activates targeted photodynamic destruction of leukaemic cells. *Br. J.*
724 *Cancer* **95**, 189-196 (2006).
725 37 Rose, A.L. & Waite, T.D. Chemiluminescence of luminol in the presence of iron(II) and
726 oxygen: Oxidation mechanism and implications for its analytical use. *Anal. Chem.* **73**,
727 5909-5920 (2001).
728 38 Thorpe, G.H.G., Kricka, L.J., Moseley, S.B. & Whitehead, T.P. Phenols as Enhancers of
729 the Chemi-Luminescent Horseradish-Peroxidase Luminol Hydrogen-Peroxide Reaction -

Application in Luminescence-Monitored Enzyme Immunoassays. *Clin. Chem.* **31**, 1335-1341 (1985).

39 Sidhu, A.B.S., Verdier-Pinard, D. & Fidock, D.A. Chloroquine resistance in Plasmodium falciparum malaria parasites conferred by pfcrt mutations. *Science* **298**, 210-213 (2002).

40 Meshnick, S.R. Artemisinin: mechanisms of action, resistance and toxicity. *Int. J. Parasitol.* **32**, 1655-1660 (2002).

41 Green, M.D., Mount, D.L., Todd, G.D. & Capomacchia, A.C. Chemiluminescent Detection of Artemisinin - Novel Endoperoxide Analysis Using Luminol without Hydrogen-Peroxide. *J. Chromatogr.* **695**, 237-242 (1995).

42 MacRae, J.I. *et al.* Mitochondrial metabolism of sexual and asexual blood stages of the malaria parasite Plasmodium falciparum. *BMC Biol.* **11**, 67-77 (2013).

43 Park, Y.H. *et al.* High-resolution metabolomics to discover potential parasite-specific biomarkers in a Plasmodium falciparum erythrocytic stage culture system. *Malar. J.* **14** (2015).

44 Yu, M. *et al.* The Fatty Acid Biosynthesis Enzyme Fabl Plays a Key Role in the Development of Liver-Stage Malarial Parasites. *Cell Host Microbe* **4**, 567-578 (2008).

45 Sturm, A., Mollard, V., Cozijnsen, A., Goodman, C.D. & McFadden, G.I. Mitochondrial ATP synthase is dispensable in blood-stage Plasmodium berghei rodent malaria but essential in the mosquito phase. *Proc. Natl. Acad. Sci. U. S. A.* (2015).

46 Daily, J.P. *et al.* Distinct physiological states of Plasmodium falciparum in malaria-infected patients. *Nature* **450**, 1091-1095 (2007).

47 Zhang, J.L. *et al.* A LC-MS/MS method for the specific, sensitive, and simultaneous quantification of 5-aminolevulinic acid and porphobilinogen. *J. Chromatogr. B* **879**, 2389-2396 (2011).

48 Padmanaban, G., Nagaraj, V.A. & Rangarajan, P.N. An alternative model for heme biosynthesis in the malarial parasite. *Trends Biochem. Sci.* **32**, 443-449 (2007).

49 Larkin, T. & Gannicliffe, C. Illuminating the health and safety of luminol. *Sci. Justice* **48**, 71-75 (2008).

50 Bissonnette, R., Zeng, H.S., McLean, D.I., Korbelik, M. & Lui, H. Oral aminolevulinic acid induces protoporphyrin IX fluorescence in psoriatic plaques and peripheral blood cells. *Photochem. Photobiol.* **74**, 339-345 (2001).

51 Gordi, T. & Lepist, E.I. Artemisinin derivatives: toxic for laboratory animals, safe for humans? *Toxicol. Lett.* **147**, 99-107 (2004).

52 Dalton, J.T. *et al.* Clinical pharmacokinetics of 5-aminolevulinic acid in healthy volunteers and patients at high risk for recurrent bladder cancer. *J. Pharmacol. Exp. Ther.* **301**, 507-512 (2002).

53 Nakase, I., Lai, H., Singh, N.P. & Sasaki, T. Anticancer properties of artemisinin derivatives and their targeted delivery by transferrin conjugation. *Int. J. Pharm.* **354**, 28-33 (2008).

54 Sigala, P.A., Crowley, J.R., Hsieh, S., Henderson, J.P. & Goldberg, D.E. Direct Tests of Enzymatic Heme Degradation by the Malaria Parasite Plasmodium falciparum. *J. Biol. Chem.* **287**, 37793-37807 (2012).

55 Tonkin, C.J. *et al.* Localization of organellar proteins in *Plasmodium falciparum* using a novel set of transfection vectors and a new immunofluorescence fixation method. *Mol. Biochem. Parasitol.* **137**, 13-21 (2004).

775 56 Ponpuak, M. *et al.* A role for falcilysin in transit peptide degradation in the *Plasmodium*
776 *falciparum* apicoplast. *Mol. Microbiol.* **63**, 314-334 (2007).
777 57 Muralidharan, V., Oksman, A., Pal, P., Lindquist, S. & Goldberg, D.E. Plasmodium
778 falciparum heat shock protein 110 stabilizes the asparagine repeat-rich parasite proteome
779 during malarial fevers. *Nat. Commun.* **3** (2012).
780 58 Balu, B., Shoue, D.A., Fraser, M.J. & Adams, J.H. High-efficiency transformation of
781 Plasmodium falciparum by the lepidopteran transposable element piggyBac. *Proc. Natl.*
782 *Acad. Sci. U. S. A.* **102**, 16391-16396 (2005).
783 59 Klemba, M., Beatty, W., Gluzman, I. & Goldberg, D.E. Trafficking of plasmepsin II to
784 the food vacuole of the malaria parasite *Plasmodium falciparum*. *J. Cell Biol.* **164**, 47-56
785 (2004).
786 60 Straimer, J. *et al.* Site-specific genome editing in Plasmodium falciparum using
787 engineered zinc-finger nucleases. *Nat. Methods* **9**, 993-+ (2012).
788 61 Ganesan, S.M. *et al.* Yeast dihydroorotate dehydrogenase as a new selectable marker for
789 *Plasmodium falciparum* transfection. *Mol. Biochem. Parasitol.* **177**, 29-34 (2011).
790 62 Liu, J., Gluzman, I.Y., Drew, M.E. & Goldberg, D.E. The role of Plasmodium falciparum
791 food vacuole plasmepsins. *J. Biol. Chem.* **280**, 1432-1437 (2005).
792 63 Waller, R.F., Reed, M.B., Cowman, A.F. & McFadden, G.I. Protein trafficking to the
793 plastid of *Plasmodium falciparum* is via the secretory pathway. *EMBO J.* **19**, 1794-1802
794 (2000).
795

796

797 **Figure Titles and Legends**

798 **Figure 1. Exogenous ALA stimulates protoporphyrin IX biosynthesis in *Plasmodium*-**
799 **infected erythrocytes. (a)** Schematic depiction of the heme biosynthesis pathway in *P.*
800 *falciparum* parasites. Enzymes abbreviations are in red and pathway substrates and intermediates
801 are in black: ALAS (aminolevulinic acid synthase), ALAD (aminolevulinic acid dehydratase),
802 PBGD (porphobilinogen deaminase), UROS (uroporphyrinogen synthase), UROD
803 (uroporphyrinogen decarboxylase), CPO (coproporphyrinogen III oxidase), PPO
804 (protoporphyrinogen IX oxidase), FC (ferrochelatase). For simplicity, all organelles are depicted
805 with single membranes. Succinylacetone (SA) inhibits ALAD. **(b)** Bright field and fluorescence
806 microscopy images of untreated and 200 μM ALA-treated parasites. Fluorescence images were
807 acquired with a Zeiss filter set 43 HE (excitation 537-562 nm, emission 570-640 nm). **(c)** Growth

808 of asynchronous 3D7 parasites in the presence or absence of 200 μM ALA and 50 μM
809 succinylacetone (SA), with 2-minute exposures to white light on an overhead projector on days
810 0-2. Parasitemia (percentage of total erythrocytes infected with parasites) as a function of time
811 was fit with an exponential growth equation.
812
813 **Figure 2. Heme biosynthesis in infected erythrocytes persists despite disruption of parasite**
814 **enzymes or the apicoplast. (a)** LC-MS/MS detection of ^{13}C-labelled heme, PPIX, and CPP in
815 parasites grown in 200 μM 5-[$^{13}C_4$]-ALA. Parasites were extracted in DMSO, supplemented
816 with deuteroporphyrin as an internal standard, and analyzed by LC-MS/MS. Integrated analyte
817 peak areas were normalized to PPIX in each sample. RBC: uninfected red blood cells, WT:
818 parental clone 3D7, IPP/dox: isopentenyl pyrophosphate/doxycycline-treated 3D7 parasites. **(b-**
819 **c)** Growth of asynchronous ΔPBGD **(b)** and ΔCPO **(c)** 3D7 parasites in the presence or absence
820 of 200 μM ALA, with 2-minute light exposures on an overhead projector on days 0-2. WT
821 growth was fit to an exponential equation. **(d)** Bright field and fluorescence images of live 3D7
822 parasites expressing ALAD-GFP from a plasmid before or after two-week treatment with IPP
823 and doxycycline. **(e)** Growth of asynchronous IPP/doxycycline-treated parasites in the presence
824 or absence of 200 μM ALA and 50 μM succinylacetone (SA), with 2-minute light exposures on
825 an overhead projector on days 0-2.
826
827 **Figure 3. Erythrocytes have latent porphyrin biosynthesis activity that requires exogenous**
828 **ALA and parasite permeability mechanisms to enable ALA uptake. (a)** LC-MS/MS
829 detection of ^{13}C-labelled PPIX and CPP in erythrocyte lysate supernatants incubated with 200
830 μM 5-[$^{13}C_4$]-ALA without or with 50 μM succinylacetone (SA). Erythrocytes were lysed in

831 0.04% saponin, centrifuged at 25,000 x g for 60 min., and 0.2 μM syringe filtered prior to ALA
832 addition. **(b)** Bright field and fluorescence (Zeiss filter set 43 HE) images of uninfected
833 erythrocytes incubated in 500 μM ALA before or after electroporation. **(c)** Bright field and
834 fluorescence images of parasites cultured in 500 μM ALA with normal (+TMP) or blocked (-
835 TMP) establishment of parasite permeability pathways in the erythrocyte membrane. Infected
836 erythrocyte permeability was modulated using a 3D7 parasite line expressing HSP101 tagged at
837 its endogenous locus with a trimethoprim (TMP)-dependent destabilization domain.[27] TMP was
838 maintained or washed out from synchronous schizont-stage parasites, which were allowed to
839 rupture and invade new erythrocytes. 500 μM ALA was added to both cultures after invasion,
840 and parasites were imaged 8 hours later.
841
842 **Figure 4. Schematic depiction of ALA-uptake and porphyrin biosynthesis pathways in**
843 ***Plasmodium*-infected erythrocytes.** For simplicity, all membranes are depicted as single.
844 Porphyrins synthesized in the infected erythrocyte cytoplasm from exogenous ALA may be
845 transported across the parasite membrane via unspecified mechanisms or may be taken up via
846 hemoglobin import mechanisms. Succinylacetone (SA) inhibits ALAD and blocks porphyrin
847 synthesis from ALA.
848
849 **Figure 5. Analysis of heme biosynthesis activity in parasite-infected erythrocytes after**
850 **saponin permeabilization and culture in ^{13}C-labelled ALA. (a)** Parasite-infected erythrocytes
851 were permeabilized in 0.02% saponin, washed to remove the erythrocyte cytoplasm, and placed
852 back into culture medium containing 200 μM 5-[$^{13}C_4$]-ALA for 12 hours prior to DMSO
853 extraction and analysis by LC-MS/MS. Bright field and fluorescence image of live **(b)** asexual

854 trophozoite and **(c)** stage IV sexual gametocyte treated with 0.02% saponin and stained with 20
855 nM Mitotracker Red. **(d)** LC-MS/MS quantification of ^{13}C-labelled heme, PPIX, and CPP in
856 DMSO extracts of intact WT 3D7 asexual parasites, saponin-released asexual parasites, and
857 saponin-released gametocytes cultured overnight in 200 μM 5-[$^{13}C_4$]-ALA.
858
859 **Figure 6. Analysis of heme biosynthetic flux within the apicoplast of live parasites using the**
860 **cobA biosensor. (a)** Fluorescence excitation (black) and emission (red) spectra of clarified
861 lysates from *E. coli* bacteria expressing the cobA gene from *Propionibacterium freudenreichii*
862 (*shermanii*), showing the expected peaks for conversion of uroporphyrinogen III to
863 sirohydrochlorin and trimethylpyrrocorphin. **(b)** Fluorescence microscopy images of live bacteria
864 expressing the cobA gene, acquired on the bright field and red (Zeiss filter set 43 HE) channels.
865 **(c)** Immunofluorescence images of fixed 3D7 parasites episomally expressing an ACP_{leader}-
866 cobA-GFP fusion confirm targeting to the parasite apicoplast. Parasites were stained with αGFP
867 and αACP (acyl carrier protein, apicoplast marker). The αACP antibody recognizes an epitope
868 that is different from the ACP leader sequence. **(d)** Fluorescence microscopy images of live
869 asexual parasites episomally expressing ACP_{leader}-cobA-GFP without or with 500 μM exogenous
870 ALA. **(e)** Fluorescence microscopy images of live stage III-IV sexual gametocytes episomally
871 expressing ACP_{leader}-cobA-GFP without or with 500 μM exogenous ALA. Fluorescence images
872 in **(d)** and **(e)** were acquired on the GFP (Zeiss filter set 38) and red (Zeiss filter set 43 HE)
873 channels.
874
875 **Figure 7. Targeting blood-stage *Plasmodium* parasites by chemiluminescence-based**
876 **photodynamic therapy (CL-PDT). (a)** Schematic depiction of a CL-PDT mechanism for

targeting blood-stage malaria. **(b)** Effect of 100 μM ALA, 750 μM luminol (lum), 50 μM 4-iodophenol (ph), 50 μM succinylacetone (SA) and their combination (all 0.25% DMSO) on the growth of asynchronous 3D7 parasites. **(c)** Effect of 100 μM ALA, 750 μM luminol, 0.5 nM dihydroartemisinin (DHA), 50 μM succinylacetone (SA) and their combination (all 0.25% DMSO) on the growth of asynchronous 3D7 parasites. Parasite media was changed twice daily, and parasitemia increases were fit to an exponential growth equation.

Video Titles and Legends

Video 1. Hemozoin dynamics in the digestive vacuole of untreated parasites prior to 4-sec. acquisitions with the Zeiss filter sets 38 (excitation 450-490 nm) and 43 HE (excitation 537-562 nm). Time-lapse bright field images were acquired with 1 sec. delays and played back with 0.1 sec. delays between frames.

Video 2. Hemozoin dynamics in the digestive vacuole of untreated parasites are unaffected by 4-sec. acquisitions with the Zeiss filter sets 38 (excitation 450-490 nm) and 43 HE (excitation 537-562 nm). Time-lapse bright field images were acquired with 1 sec. delays and played back with 0.1 sec. delays between frames. Bright field images were acquired before and after 4 sec. image acquisitions with the Zeiss filter sets 38 (excitation 450-490 nm) and 43 HE (excitation 537-562 nm).

Video 3. Hemozoin dynamics in the digestive vacuole of 200 μM ALA-treated parasites prior to 4-sec. acquisitions with the Zeiss filter sets 38 (excitation 450-490 nm) and 43 HE

(excitation 537-562 nm). Time-lapse bright field images were acquired with 1 sec. delays and played back with 0.1 sec. delays between frames.

Video 4. Hemozoin dynamics in the digestive vacuole of 200 µM ALA-treated parasites are ablated after 4-sec. acquisitions with the Zeiss filter sets 38 (excitation 450-490 nm) and 43 HE (excitation 537-562 nm). Time-lapse bright field images were acquired with 1 sec. delays and played back with 0.1 sec. delays between frames. Bright field images were acquired before and after 4 sec. image acquisitions with the Zeiss filter sets 38 (excitation 450-490 nm) and 43 HE (excitation 537-562 nm).

Figure Supplement Titles and Legends

Figure 1- figure supplement 1. Fluorescence excitation and emission spectrum of protoporphyrin IX in aqueous buffer.

Figure 1- figure supplement 2. Transmission electron microscopy images of untreated and 500 µM ALA-treated *P. falciparum*-infected erythrocytes after light exposure on an overhead projector light box. The white arrow identifies the digestive vacuole. Scale bar equals 1 µm.

Figure 1- figure supplement 3. ALA-dose dependence of photosensitivity by blood-stage *Plasmodium* parasites. Asynchronous parasites were cultured in the indicated concentration of ALA and exposed to 2 min. light daily. Parasitemia was measured after 48 hours and normalized to a reference culture grown without ALA.

Figure 1- figure supplement 4. Giemsa-stained blood smear of *P. falciparum* culture after three days of treatment with 200 µM ALA and 2-min. daily light exposure on an overhead projector light box. Black arrows identify dead parasite remnants.

Figure 2- figure supplement 1. Immunofluorescence images of fixed 3D7 parasites expressing full-length PBGD tagged at its endogenous locus with C-terminal GFP confirm targeting of the native protein to the parasite apicoplast. Parasites were stained with αGFP and αACP (acyl carrier protein, apicoplast marker).

Figure 2- figure supplement 2. Fluorescence microscopy images of live 3D7 parasites episomally expressing full-length CPO with a C-terminal GFP tag confirm protein localization to the parasite cytoplasm.

Figure 2- figure supplement 3. Disruption of the *P. falciparum* porphobilinogen deaminase (PBGD) gene (PF3D7_1209600) by single-crossover homologous recombination. (a) Schematic depiction of the PBGD gene locus before and after incorporation of the donor plasmid via single-crossover recombination. Red arrows indicate the primers used to selectively PCR-amplify either the intact WT or disrupted ΔPBGD locus. SacI and BglII were used to digest the donor plasmid and gDNA of WT and ΔPBGD parasites to give the expected fragment sizes indicated in parentheses for hybridization to a PBGD bp 601-960 oligonucleotide probe. **(b)** PCR analysis of gDNA from WT and ΔPBGD clones using the primers indicated in **(a)** to selectively amplify the 1.3 kb WT gene or the 960 bp truncated gene. **(c)** Southern blot analysis of gDNA

945 from 3D7 WT and ΔPBGD clonal parasites after digestion with SacI and BglII, hybridization
946 with a PBGD bp 601-960 oligonucleotide probe, and detection using the Amersham AlkPhos
947 Labeling and CDP-Star Chemiluminescent reagents. **(d)** Homology model of *P. falciparum*
948 PBGD (human PBGD template structure 3EQ1) to indicate the portion of the protein retained
949 (cyan) or lost (green) by single-crossover truncation. The deleted sequence comprises half of the
950 active site binding pocket, identified by the dipyrromethane cofactor shown in red.
951
952 **Figure 2- figure supplement 4. Disruption of the *P. falciparum* coproporphyrinogen III**
953 **oxidase (CPO) gene (PF3D7_1142400) by single-crossover homologous recombination. (a)**
954 Schematic depiction of the CPO gene locus before and after incorporation of the donor plasmid
955 via single-crossover recombination. Red arrows indicate the primers used to selectively PCR-
956 amplify either the intact WT or disrupted ΔCPO locus. XhoI and KpnI were used to digest the
957 donor plasmid and gDNA of WT and ΔCPO parasites to give the expected fragment sizes
958 indicated in parentheses for hybridization to a CPO bp 610-1080 oligonucleotide probe. **(b)** PCR
959 analysis of gDNA from WT and ΔCPO clones using the primers indicated in **(a)** to selectively
960 amplify the 1.6 kb WT gene or the 1.1 kb truncated gene. **(c)** Southern blot analysis of gDNA
961 from 3D7 WT and ΔCPO clonal parasites after digestion with XhoI and KpnI, hybridization with
962 a CPO bp 610-1080 oligonucleotide probe, and detection using the Amersham AlkPhos Labeling
963 and CDP-Star Chemiluminescent reagents. **(d)** Homology model of *P. falciparum* CPO (human
964 CPO template structure 2AEX) to indicate the portion of the protein retained (blue) or lost
965 (green) by single-crossover truncation. The deleted sequence comprises half of the active site
966 binding pocket, identified by the citrate molecule shown in red.
967

Figure 2- figure supplement 5. Immunofluorescence images of fixed 3D7 parasites expressing full-length ALAD tagged at its endogenous locus with C-terminal GFP confirm targeting to the parasite apicoplast. Parasites were stained with αGFP and αACP (acyl carrier protein, apicoplast marker).

Figure 2- figure supplement 6. PCR analysis of genomic DNA from untreated WT parasites or parasites cultures ≥7 days in 1 μM doxycycline and 200 μM isopentenylpyrophosphate (IPP). ACP_L refers to the 385 bp leader sequence (with introns) of the nuclear-encoded acyl carrier protein. Rps8 (387 bp) and ORF91 (276) are two genes encoded by the *Plasmodium* apicoplast genome.

Figure 2- figure supplement 7. Western blot analysis of parasites episomally expressing ALAD-GFP and cultured 7 days in IPP and doxycycline. Blots confirm disrupted proteolytic processing of the ALAD leader sequence that results in retarded migration by SDS-PAGE relative to parasites cultured in normal conditions. Extracts from WT and IPP/doxycycline parasites were loaded separately in lanes 2 and 5, respectively, and were loaded together in lanes 3 and 4.

Figure 3- figure supplement 1. Furosemide blocks ALA uptake and PPIX biosynthesis in parasite-infected erythrocytes. Asynchronous wild-type 3D7 parasites were incubated in the absence or presence of 100 μM furosemide for one hour to block nutrient acquisition pathways, followed by addition of 500 μM ALA and further incubation for eight hours. Parasites were then

990 imaged by live microscopy on the bright field or red fluorescence (Zeiss filter set 43 HE)
991 channels. In lower panel**,** parasite nuclei (blue) were visualized with Hoechst DNA stain.
992

993 **Figure 4- figure supplement 1. Growth of parasites in 1 μM 5-[$^{13}C_4$]-ALA results in**
994 **detectable biosynthesis of ^{13}C-labeled PPIX.** Parasites were grown overnight in 1 μM 5-[$^{13}C_4$]-
995 ALA, permeabilized with saponin, extracted in DMSO, and analyzed by LC-MS/MS for ^{13}C-
996 labeled heme, PPIX, and CPP. Integrated peak areas measured for each analyze were normalized
997 to that measured for the deuteroporphyrin internal standard added to each sample.
998

999 **Figure 6- figure supplement 1. Disruption of the ferrochelatase gene in ΔFC parasites does**
1000 **not photosensitize parasites.** WT or ΔFC D10 parasites were cultured under normal growth
1001 conditions (without exogenous ALA) with two-minute light exposures on an overhead projector
1002 light box on days 0-2. Culture parasitemia as a function of time was fit to an exponential growth
1003 model. Both WT and ΔFC parasites had parasitemia doubling times of 1.1 days under these
1004 conditions.
1005

1006 **Figure 7- figure supplement 1. Spectral compatibility of luminol and PPIX. (a)** Overlay of
1007 normalized absorbance spectrum of PPIX (black) and chemiluminescence spectrum of luminol
1008 (red). **(b)** Chemiluminescence of luminol (solid red) is attenuated in the presence of PPIX (solid
1009 black), giving rise to a difference spectrum (dashed black) that is similar to the absorbance
1010 spectrum of PPIX in the spectral region that overlaps luminol chemiluminescence. Solutions
1011 contained 25 mM luminol in 100 mM NaOH (aq), 0.5% (w/v) ammonium persulfate, and/or 70
1012 μM PPIX.

Figure 7- figure supplement 2. Effect of combinatorial ALA, luminol, and 4-iodophenol on parasite growth. (a) Luminol concentrations as high as 750 μM (in 0.2% DMSO) have no effect on 3D7 parasite growth over 48 hours. **(b)** Effect of 750 μM luminol, 100 μM ALA, and their combination (all in 0.2% DMSO) on the growth of asynchronous 3D7 parasites. **(c)** Concentration dependence of growth inhibition of 3D7 parasites by 4-iodophenol (in 0.2% DMSO) over 48 hours. **(d)** Effect of 100 μM ALA, 50 μM 4-iodophenol, and their combination (all in 0.2% DMSO) on the growth of asynchronous 3D7 parasites.

Figure 7- figure supplement 3. Giemsa-stained blood smear of 3D7 parasite culture after 3 days of treatment in 100 μM ALA, 750 μM luminol, and 50 μM 4-iodophenol. Arrows point to dead parasite remnants.

Figure 7- figure supplement 4. Efficacy of chemiluminescence-based photodynamic therapy with drug-resistant parasites. Effect of 100 μM ALA, 750 μM luminol, 50 μM 4-iodophenol, 50 μM succinylacetone (all 0.2% DMSO) and their combination on the growth of asynchronous **(a)** Dd2 parasites or **(b)** Kelch-13 I543T (MRA-1241) parasites.

Figure 7- figure supplement 5. Concentration dependence of growth inhibition of 3D7 parasites by dihydroartemisinin (DHA) over 48 hours (in 0.2% DMSO).

Figure 7- figure supplement 6. Effect of 500 pM DHA, 100 μM ALA, and their combination (all in 0.2% DMSO) on the growth of asynchronous 3D7 parasites.

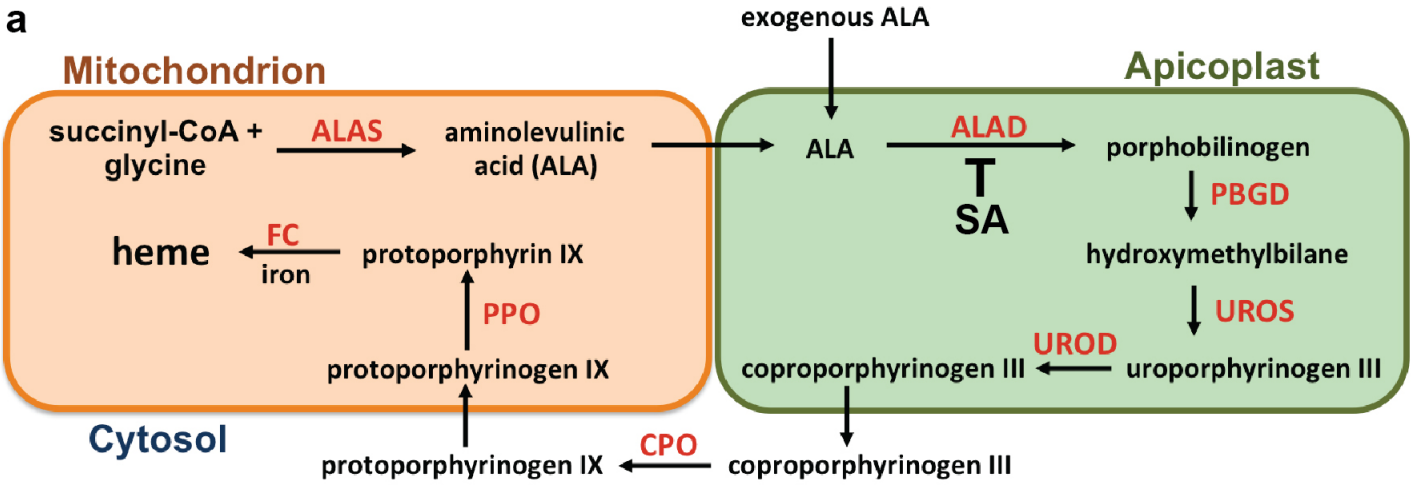
a
exogenous ALA
Mitochondrion
Apicoplast
succinyl-CoA + glycine
ALAS
aminolevulinic acid (ALA)
ALA
ALAD
T
SA
porphobilinogen
PBGD
hydroxymethylbilane
UROS
heme
FC
iron
protoporphyrin IX
PPO
protoporphyrinogen IX
UROD
coproporphyrinogen III
uroporphyrinogen III
Cytosol
protoporphyrinogen IX
CPO
coproporphyrinogen III

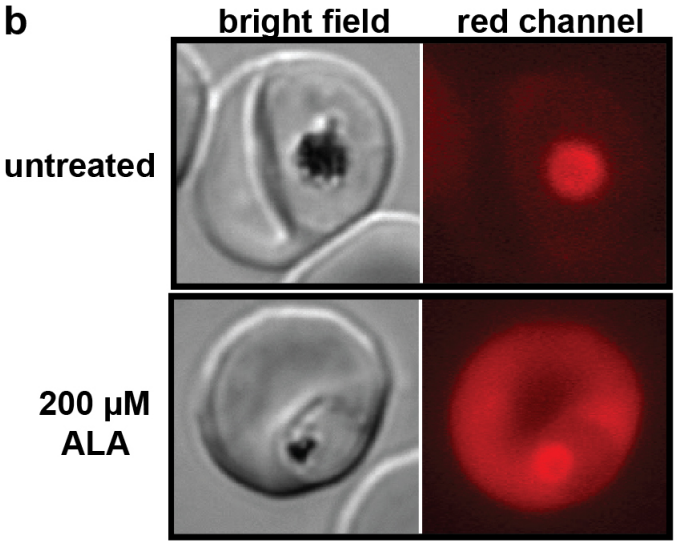
b
bright field
red channel
untreated
200 µM ALA

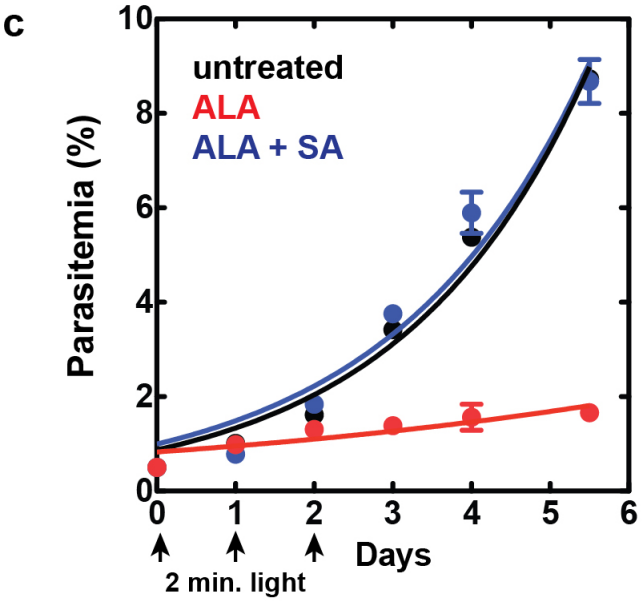
c
untreated
ALA
ALA + SA
Parasitemia (%)
0
2
4
6
8
10
0
1
2
3
4
5
6
Days
2 min. light

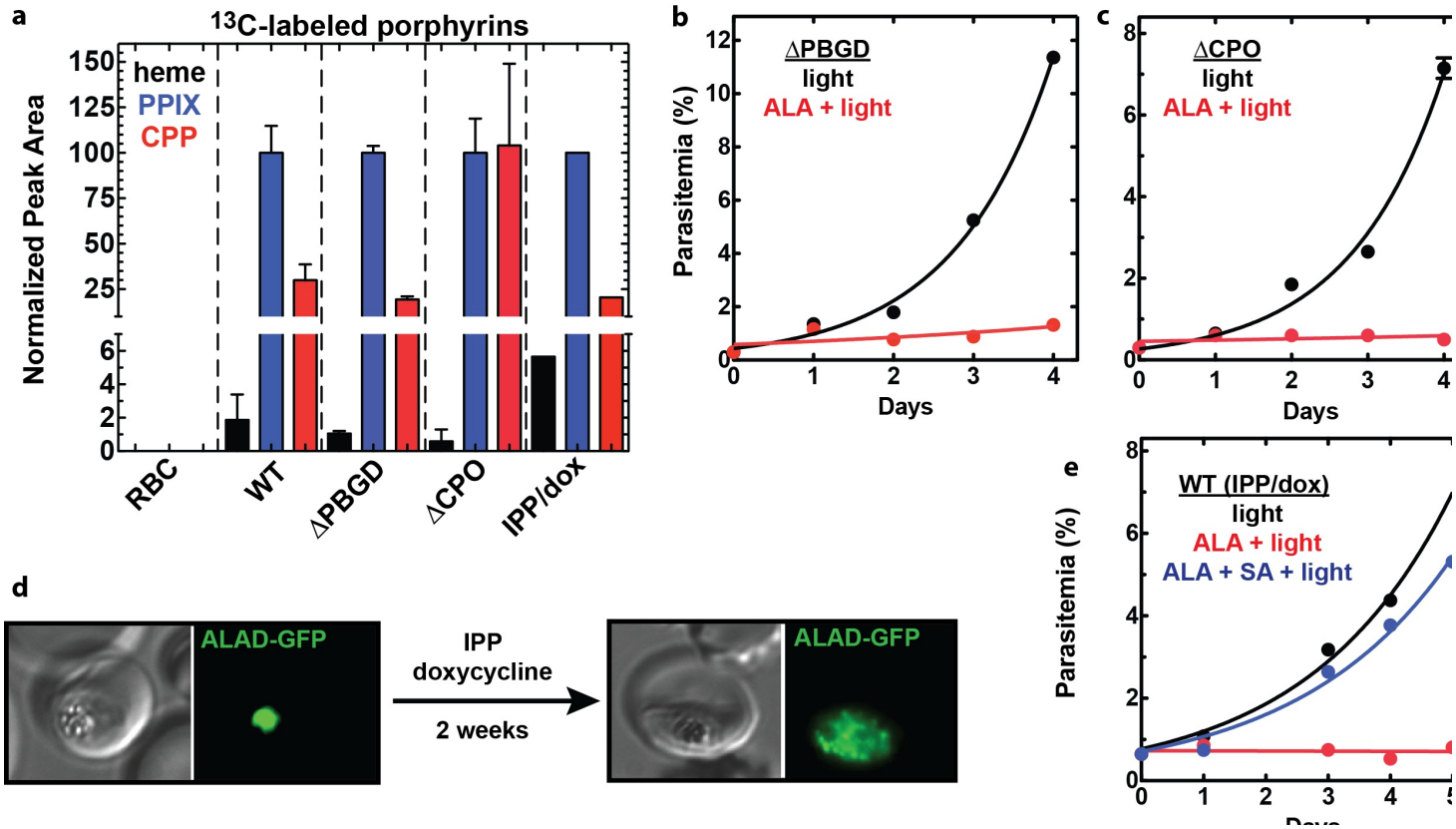
a
^{13}C-labeled porphyrins
Normalized Peak Area
heme
PPIX
CPP
RBC
WT
ΔPBGD
ΔCPO
IPP/dox
b
ΔPBGD
light
ALA + light
Parasitemia (%)
Days
c
ΔCPO
light
ALA + light
Days
d
ALAD-GFP
IPP
doxycycline
2 weeks
ALAD-GFP
e
WT (IPP/dox)
light
ALA + light
ALA + SA + light
Parasitemia (%)

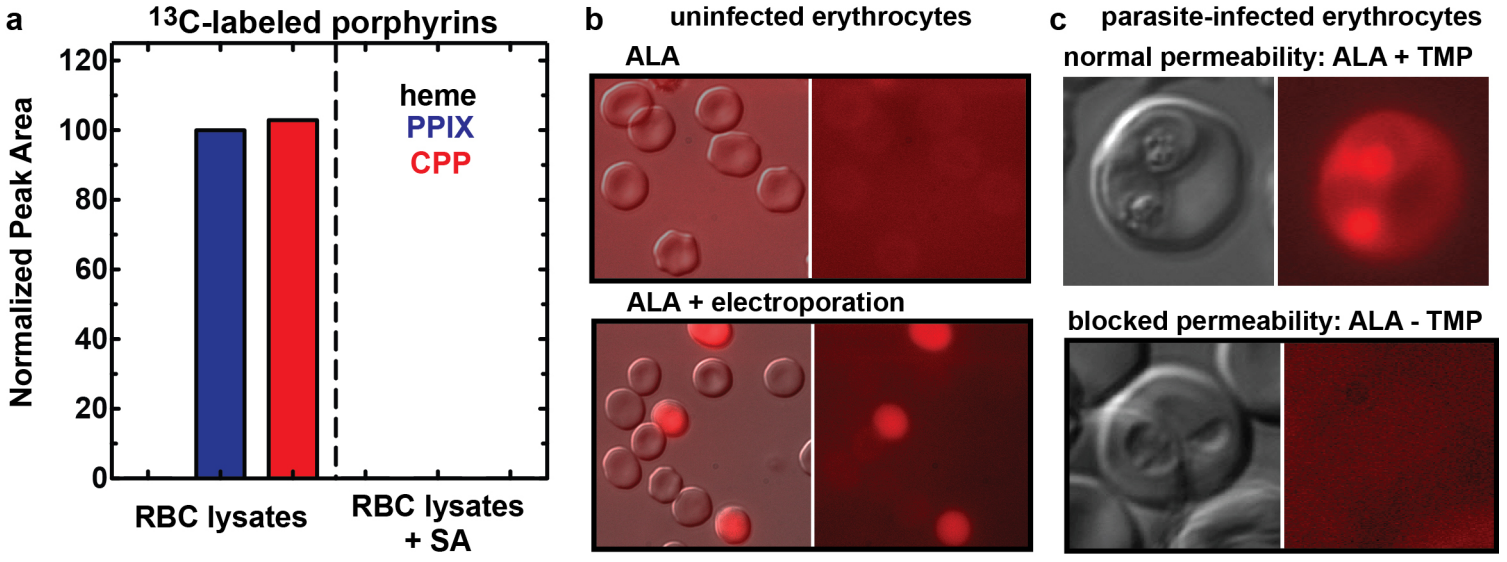
a
^{13}C-labeled porphyrins
Normalized Peak Area
120
100
80
60
40
20
0
heme
PPIX
CPP
RBC lysates
RBC lysates
+ SA
b
uninfected erythrocytes
ALA
ALA + electroporation
c
parasite-infected erythrocytes
normal permeability: ALA + TMP
blocked permeability: ALA - TMP

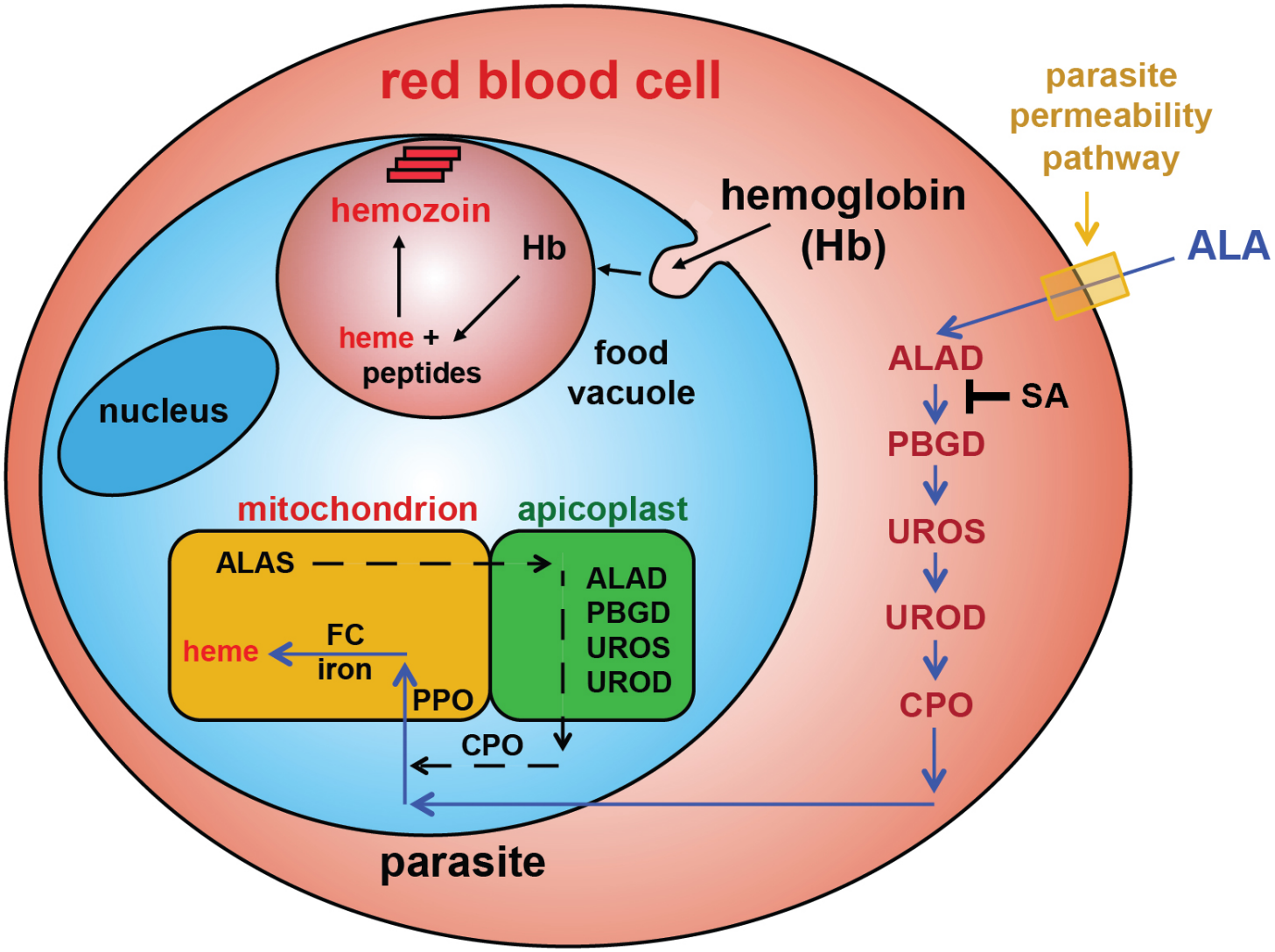
red blood cell
parasite permeability pathway
ALA
hemoglobin (Hb)
hemozoin
Hb
heme + peptides
food vacuole
nucleus
ALAD
SA
PBGD
UROS
UROD
CPO
mitochondrion
apicoplast
ALAS
ALAD
PBGD
UROS
UROD
heme
FC
iron
PPO
CPO
parasite

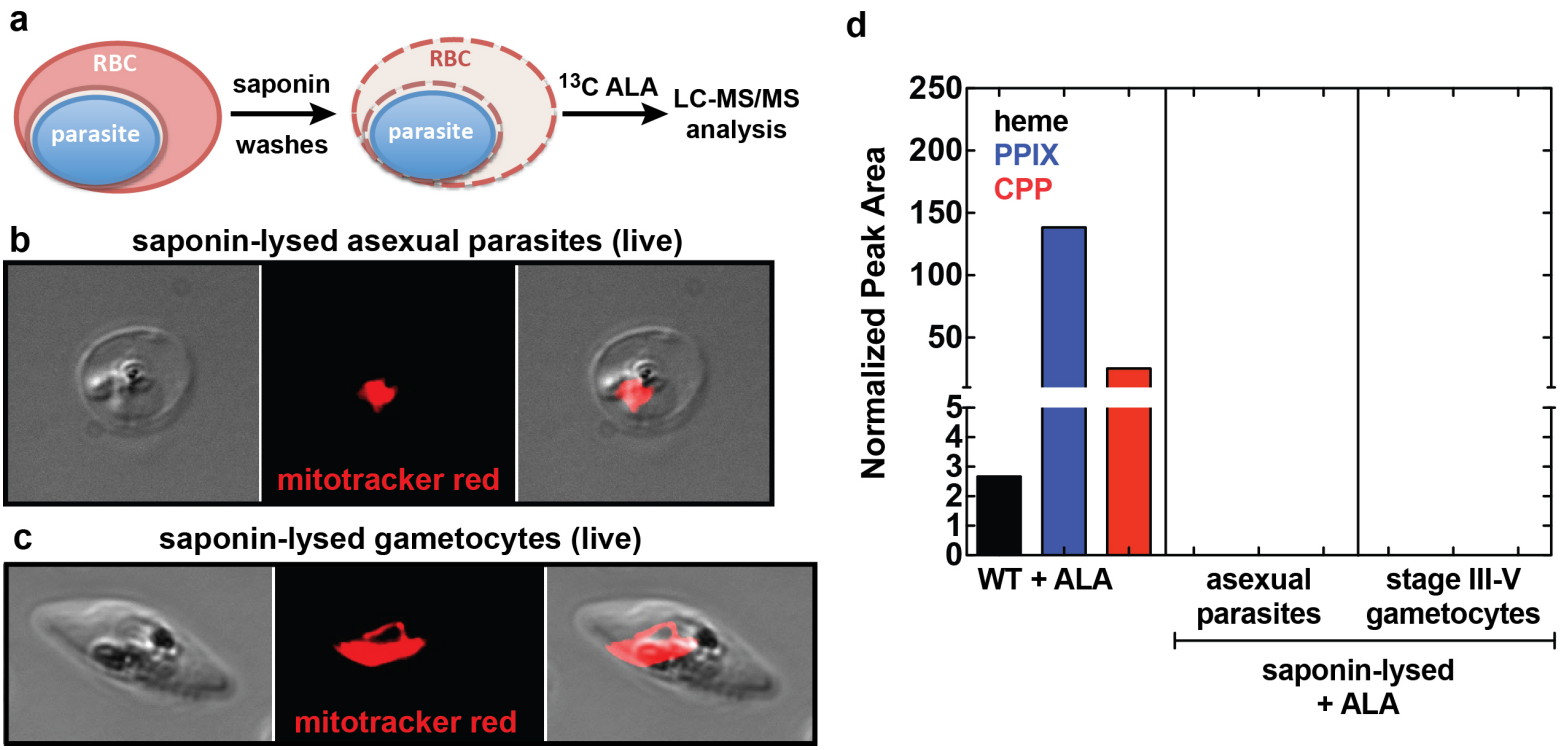
a
RBC
parasite
saponin
washes
RBC
parasite
^{13}C ALA
LC-MS/MS
analysis
b
saponin-lysed asexual parasites (live)
mitotracker red
c
saponin-lysed gametocytes (live)
mitotracker red
d
Normalized Peak Area
250
200
150
100
50
5
4
3
2
1
0
heme
PPIX
CPP
WT + ALA
asexual
parasites
stage III-V
gametocytes
saponin-lysed
+ ALA

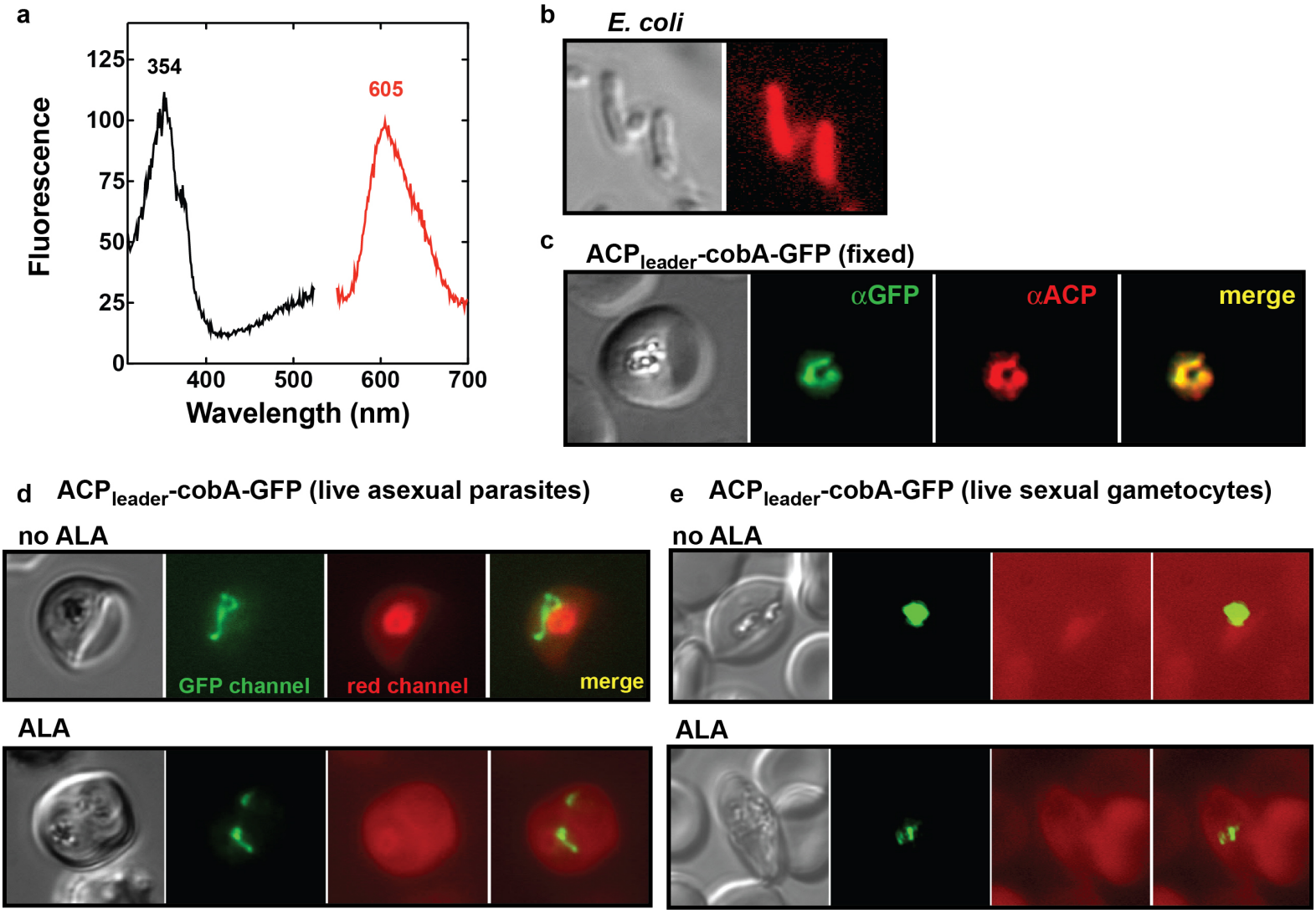
a
Fluorescence
125
100
75
50
25
0
354
605
400
500
600
700
Wavelength (nm)
b
E. coli
c
ACPleader-cobA-GFP (fixed)
αGFP
αACP
merge
d
ACPleader-cobA-GFP (live asexual parasites)
no ALA
GFP channel
red channel
merge
ALA
e
ACPleader-cobA-GFP (live sexual gametocytes)
no ALA
ALA

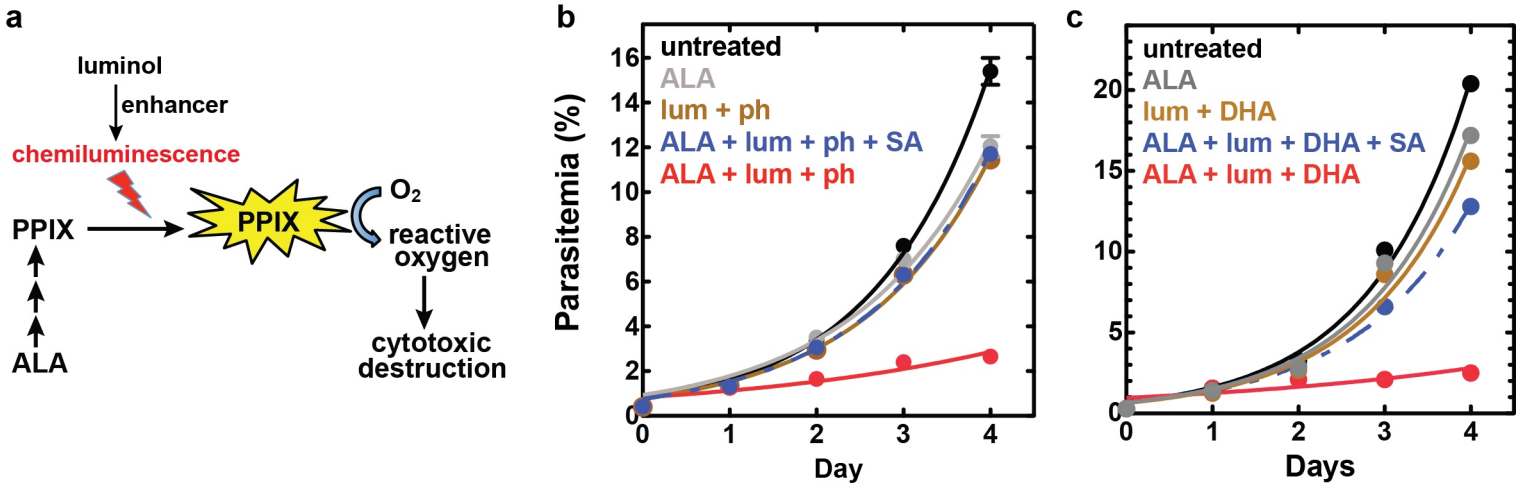
a
luminol
enhancer
chemiluminescence
PPIX
PPIX
O2
reactive oxygen
cytotoxic destruction
ALA
b
untreated
ALA
lum + ph
ALA + lum + ph + SA
ALA + lum + ph
Parasitemia (%)
Day
c
untreated
ALA
lum + DHA
ALA + lum + DHA + SA
ALA + lum + DHA
Days